PHASE FIELD MODELLING OF FRACTURE PROPERTIES FROM SCRATCH TEST

A Thesis

by

ATUL VAIBHAV

Submitted to the Office of Graduate and Professional Studies of
Texas A&M University
in partial fulfillment of the requirements for the degree of

MASTER OF SCIENCE

Chair of Committee,	Arash Noshadravan
Committee Members,	J.N. Reddy
	Minsu Cha
Head of Department,	Robin Autenrieth

August 2019

Major Subject: Civil Engineering

ABSTRACT

Scratch test is one of the oldest concepts for characterizing mechanical properties of a material. The inference of the relationship between scratch force and material property is still a contemporary topic in applied mechanics. It has applications ranging from assessment of wear of metals and strength of rocks to skin biomechanics and the recent nanoscale evaluation of scratch damage in polymers. Despite the seeming simplicity of the procedure, a fundamental understanding of the underlying mechanism remains indistinct. The complexity lies with the prediction of mechanism that drives the scratch resistance, i.e. the chipping of material. The objective of this research is to revisit the characterization of fracture properties of shale materials from scratch test measurements. This problem of considering scratching as a fracture process has been approached through experiments and theories but there is a big gap when it comes to associate the experimental results with a computational approach which is analogous to the actual mechanism. We propose that this phenomenon can be described in a diffuse sense with a phase field approach utilizing a prescribed length scale parameter which takes the chipping off length into account. The surface energy linked to the crack propagation arising from the movement of the scratch-blade against brittle sample is evaluated using a functional expressed in terms of a scalar order parameter (phase field variable) and its gradients. This parameter is linked to the displacement problem through an energy degradation function which reflects the stiffness loss in the material volume as it suffers damage. Thus, the coupled system of partial differential equations for displacement as well as the scalar

parameter obtained from total energy minimization regulate phase field evolution and impose the stress equilibrium. These equations are solved numerically using finite element models for both the displacement and the crack phase field. The model uses experimental data of scratch test conducted on few samples of shale. Through the analysis of several numerical examples reinforced with the experimental data we validate a computational model which can be used to predict fracture property of a material and the essential failure mechanism.

ACKNOWLEDGEMENTS

I would like to express my gratitude to my committee chair, Dr. Noshadravan, and my committee members, Dr. Reddy and Dr. Cha for their guidance and support throughout the course of this research.

Thanks also go to my friends and colleagues and the department faculty and staff for making my time at Texas A&M University a wonderful experience.

Finally, thanks to my family for their encouragement and love.

CONTRIBUTORS AND FUNDING SOURCES

Contributors

This work was supervised by a thesis committee consisting of Professor Arash Noshadravan and Professor Minsu Cha of the Department of Civil Engineering and Professor J.N. Reddy of the Department of Mechanical Engineering.

The experimental data analyzed was provided by Professor Sara Abedi.

All other work conducted for the thesis was completed by the student independently.

Funding Sources

This work was completed without outside financial support.

TABLE OF CONTENTS

Page

LIST OF FIGURES

Page

LIST OF TABLES

Page

1 INTRODUCTION

1.1 Overview

Failure criteria for rocks are mostly comprised of stresses and are thus apt mainly for homogeneous state of stresses. Since in rocks that is rarely the case and we generally deal with highly inhomogeneous occurrence of stress, it is likely that the failure mechanism is affected by stress or strain gradients (Mindlin, 1963). It is also observed that brittle failure and the onset of static yielding occur at higher than expected loads such as in the case of stress concentration. In general, growing strain gradients seem to make some materials stronger and sometimes even to an extent that it starts depending upon grain size. In order to capture the microstructural effects for rocks, the course of action is to generate continuum models with microstructure or find ways to introduce length scale into the problem. Petroleum shale is one of the rocks whose properties have been under intensive study for years. Characterization and modeling of mechanical and damage properties of this reservoir rock is crucial for enhancing exploration and production from hydrocarbon reservoirs. It is also relevant in many other disciplines such as hydrology and subsurface engineering. In the context of understanding poroelastic properties, there has been promising developments over the last decade regarding multiscale characterization and modeling of shale since the pioneering work of Ulm and Abousleiman (2006). Utilizing this multiscale framework, the effect of texture, mechanical, thermal maturity, and chemical composition on poroelastic behavior of shale are studied in some recent works (Abedi et al., 2016; Monfared and Ulm, 2016). Mashhadian et al. (2018) adopted a probabilistic approach consisting of experimental characterization, micro-poromechanical

modelling and uncertainty quantification and propagation in order to improve the predictive capability in modeling multiscale poroelastic properties of undamaged shale at macroscale. The inclusion of effect of microcrack has been another recent effort to extend the multiscale modeling of shale beyond the poroelastic properties (Mashhadian et al., 2018; Dubey et al., 2018). Despite the recent developments in physics-based modeling of shales, much work remains to be done in order to expand our understanding of different mechanical properties of this complex material. In particular, the characterization and modeling of fracture properties of shale at smaller length scale is still a challenging task. Scratch test, as one of the oldest concepts for has been recently used for this purpose. Akono et al. (2011) emphasizes on how the fracture process zone expands into the bulk material without any interference from size and boundary of the specimen hence serving as a suitable alternative for this task. They produced scaled relations between applied forces and the scratch width and depth to determine the fracture toughness. They also compared this phenomenon to slicing of butter and the observed chipping during the process. Although the actual test is quite straightforward, the complexity lies with the prediction of failure mechanism that drives the scratch resistance, i.e. the chipping of material.

1.2 Research Objective

In this study we try to explain the scratch test and the apparent chipping phenomenon using the phase field method, which takes the length scale into account. Within this framework, the surface energy linked to the crack propagation arising from the movement of the scratch-blade against brittle sample is evaluated using a functional expressed using a scalar order parameter (phase field variable) and its gradients. This in succession define fractures in a dispersed manner along an imposed regularization length scale. We draw a contrast between this regularization parameter and the scratch mechanism in the background of experimental test data. Nguyen et al. (2016) talks about how changing this parameter could essentially mean changing the material. We exploit this proposition and further extend it to express a range of characteristic length scale for a given material defined by material property and the physical constraints of scratch test. Using this we determine a range of fracture toughness for that material.

1.3 Thesis Outline

This thesis is organized as follow. In Chapter 2 the details and the properties we of scratch test are discussed. The energy balance equation that governs when scratching is performed by a tool and the physical significance of chipping phenomenon is also described. Chapter 3 focuses on the main idea and formulations of phase field method. The evolution of minimization of energy principle originating from Griffith criteria for fracture mechanics is laid out. Chapter 4 describes the experiment and the data derived from scratch test. Secondly, an analytical phase field approximation to scratch test and its

relationship with experimental data is developed. This relationship is used to generate an algorithm to determine fracture toughness of a brittle material. Along with this a two-dimensional simulation of scratch test is illustrated using a phase field based finite element model. Finally, in Chapter 5, the results of this study are laid out focusing on capabilities and limitations of this approach.

2 SCRATCH TEST FOR DESCRIPTION OF MECHANICAL PROPERTIES

2.1 Background

Avoiding fracture is the primary objective when it comes to design of components and structures in engineering. But there are situations in which separation of parts is incumbent. The most common example is in manufacturing of precise surface in metals with the help of special tools for cutting. The process of separation includes both maneuvering an object at regions distant from where it breaks, to loading the objects right at the zone of fracture. Separation of materials is ubiquitous: in the kitchen (e.g. peeling vegetables, slicing butter), in carpentry and building, in manufacturing, in medicine and dentistry. While, generally deformation is not significant in the cutting tool than it is in the object unless we talk about fields like laser cutting or abrasive water jet cutting. The former is a characteristic feature of controlled cutting and we will focus on the aspect of cutting where the tool or blade is not deformed when cutting. Dissimilar materials react differently to the cutting process. It may consist of big pieces getting separated into two or thin slices/chips getting removed from the surface of a large piece. In engineering fields what is of concern is the quality of generated surfaces. The response of the specimen being cut can be recorded and can be utilized to determine a number of mechanical or physical properties. Clearly, this response would also depend on the way the cutting process is conducted and thus what mechanism or path of failure the specimen underwent. The types of cutting can be summed up as:

- indenting a groove on the surface of the body
- cutting layers from surface of the body

The difference between them is essentially the tool-material interaction that occurs and the failure mechanism that follows. Scratch test, which is an indentation or cutting experiment is the procedure where this interaction is of importance. The idea behind scratch test is cutting the surface of a weaker material with a scratch device and quantifying the hardness (H_T) of the material by the resistance it offered. The horizontal force associated with the scratch test can be expressed as

$$F_T = H_T A_{lb} \quad (1)$$

Where, F_T is the horizontal force applied by the device and A_{lb} is the projected area which resists this horizontal force. Given the simplicity in measuring the depth and force as it is progressing, scratch test is a relevant experiment for a myriad of engineering areas. It has applications ranging from assessment of wear of metals and strength of rocks to skin biomechanics and the recent nanoscale evaluation of scratch damage in polymers.

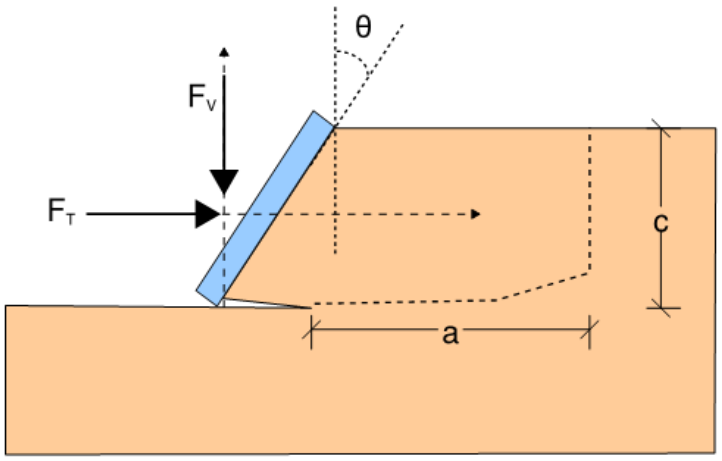

Figure 1: Scratch test setup geometry

For our case we have considered a simplified scratch test geometry (Fig (1)). A vertical force F_v is applied at an inclined angle θ to hold the blade at depth c. The forward movement of blade is controlled by the horizontal force F_T. As the blade moves while scratching, cracking takes place and the crack faces separate. This leads to a chunk of material getting removed within a chipping length a. This phenomenon of chipping and its description is something which has not been studied extensively.

2.2 Fracture Properties from Scratch Test

Over the years, indirect methods such as point load test and scratch test has been proposed as an alternative to uniaxial compression test in order to determine the compressive strength in rocks (Bieniawski, 1974, Szwedzicki, 1998).Its main advantage was assessing the strength using very small sized samples (~3-5 cm^3). The origins of using scratch test for characterization of mechanical properties of rocks can be traced back to the work done by Atkinson (1993). He asserted that rock hardness being a function of intrinsic rock properties can quantify rock strength and plastic behavior when the specific test method is provided. Adachi and Detournay (1996) presented the results of an investigation on determination of rock strength parameters from cutting tests making use of the Rock Strength Device. This approach was based on a phenomenological model interpreting the forces applied during scratching and had the ability to stipulate a record of strength from the rock cores. They considered the intrinsic specific energy, the ratio of vertical to horizontal forces applied during scratch test and the coefficient of friction between the interface to describe the induced rock failure in plastic regime. Alehossein et

al (2000) developed a method for the analysis of rock indentation by blunt indenters based on a cavity expansion model. They focused on the relationship between scratch force and the indentation depth before the tensile fracture initiates and propagates. They followed works of Marsh (1964) who suggested that the material response under the scratching tool is similar to how cylindrical and spherical cavity expands with internal pressure and Johnson (1970) who further extended this to conical indentation in a material failing under Tresca criterion. Sulem et al (2002) introduced an elasto-plastic model of rocks considering Cosserat continuum and thus possessing an internal length. They studied the response of indentation curve varying the size of indenter with respect to the internal length and assessed the scale effect. They proposed that the Cosserat theory is quite appropriate when it comes to taking the microstructural effect into account for predicting macroscopic behavior.

In addition to utilizing the scratch force-material property relationship for strength and damage evaluation, in recent years the determination of fracture properties has also been explored. When a tool induces failure of rock, it can be in a brittle manner or ductile. The brittle mode is linked with the propagation of crack which is the case of cutting while the ductile mode corresponds to advancing of a zone of damage or a plastic flow as seen in indentation. Zhu and Lin (2014) connected the transition between the ductile and brittle regime to Bazant's size effect law for brittle material. They adopted a continuum damage material model to capture this transition in rock cutting. They showed the variation of nominal stress to relative displacement with size and found the trend to be similar to single notched plates under tensile and three-point bending settings. In indentation, it has been

observed that the formation of cracks succeeds the development of damage zone. Early in the process, rock below the tool experiences crushing and compressive shear. The damage zone expands with each increment in the penetrating depth. When this zone reaches a critical size, it is followed by initiation and propagation of crack. From here on the confinement applied to specimen governs the pattern of fracture. A primary vertical appears in the absence of remote confining stress, which when stabilized leads to appearance of secondary lateral cracks. This phenomenon is reversed when a remote confining stress exists. In this case the damage region development is restricted which leads to formation of lateral cracks. These lateral cracks propagate in an unstable manner towards the free surface thus causing rock chipping and fragmentation. Richard et al (2012) studied the variation of cutting force with depth of cut in scratch test specimens. They also described a model which interprets experimental results which points that unconfined compressive strength of rocks can be assessed by scratch test. This however must be done at a depth of cut small enough so that no significant chipping of the rock is occurring.

Akono et al. (2011) developed an analytical approach to link the forces applied during scratch test to geometry of the tool and fracture properties. They considered scratch test in a linear elastic fracture mechanics framework to estimate the energy release rate by means of J integral and thus obtaining a relation between applied forces and parameters of the test to determine the fracture toughness which was validated experimentally. But when it comes to associating the experimental scratching results with a computational approach for brittle materials, there is still a gap. We propose that that this phenomenon

can be described in a diffuse sense with a phase field approach utilizing a prescribed length scale parameter and taking the depth of cut and chipping off length into account.

2.3 Mechanics Behind Chipping Length

The fashion of removal of chip (either shear or bending) and the condition it is in during or after cutting (continuous strips or discontinuous offcuts) depends on factors like material properties, geometry of the tool-blade and friction. Several techniques have been used to study the deformation pattern on chip formation. Scribing grid or circular arrays on the outer edge of the sample, observing motion of specific grains shown by chemical etching are some of the ways this is investigated. This investigation describes chip formation while cutting to fall under two separate conditions –

- Globally elastic
- Globally plastic.

Globally elastic refers to the brittle chip formation where they break off in a series of fragments accompanied with load drops. The worn-out chips can be assembled and fitted to regain the initial specimen. In case of globally plastic ductile conditions govern the continuous chip forming, with cutting under steady load. In this case whether the chips are somewhat continuous with partly cracked segments which are attached loosely or are entirely separated from one another depends on the extent of elastoplasticity during the process.

2.4 Load-Displacement Behavior in Cracked Bodies and Energy Formulation

Fracture mechanics fundamentally deals with answering the question what happens to a cracked body when it is loaded. The basic answer is cracks diminish the stiffness of the body. Longer the crack, lesser the stiffness. Looking at Fig (2.b), O-A denotes stiffness of an uncracked body. O-A1 and O-A2 represent the stiffness for cracks a_1 and a_2. It is obvious that $a_1 < a_2$. Consider that in a specimen with crack length a_1, crack starts propagating in a controlled manner at a uniform load along B-C. At the position C the crack length has reached a_2. Now, if unloading occurs the stiffness line that will followed down will be corresponding to a_2. Ultimately, the specimen will be equivalent to the one before but with a longer crack.

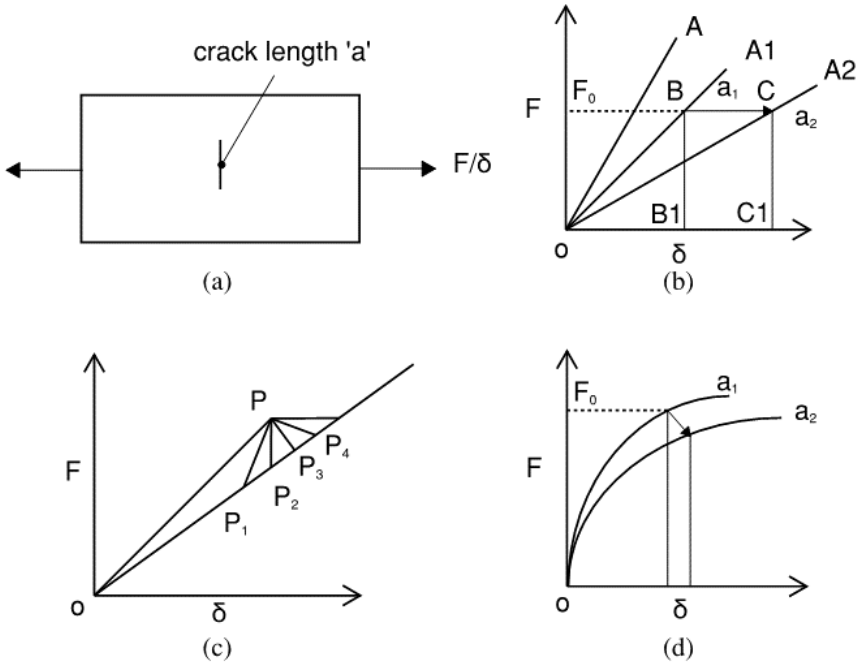

Figure 2: (a) Cracked specimen loaded with force F and displacement δ, (b) load-displacement curve for linear cracked bodies, (c) Few possible options for load paths through propagation , (d) load-displacement behavior of non-linear cracked bodies (Adapted from Atkins 2009)

Consider the balance of energy from O (F=0) to B ($F=F_0$), followed by crack propagation under this load to C($F=F_0$). After this the body is unloaded back to zero load. Up until the extension of crack, body has elastic energy stored within. This is shown by the area O-B-B1-O. When the crack propagates, the constant load imparts a displacement shown by B-C which is same as B1-C1. This advancement adds energy in the form of external work done to the body. This is given by area B-C-C1-B1. When unloading occurs, energy denoted by area O-C-C1 is retrieved. During this entire process, the energy associated with area O-B-C-O is lost. This 'lost' energy is the energy dissipated during the propagation of crack from length a_1 to a_2. This dissipated energy per unit area, also called energy release rate is G_c. The determination of this material property can be done experimentally, algebraically or using finite element methods.

Although the propagation of crack can take place under a constant loading as shown above, there are cases where it can traverse different load paths as shown in Fig (2.c). This can depend on the geometrical setup or the way loading is applied.

When cracking occurs by a tool, the general energy balance equation (Eq. 2) includes the incremental external work done converted into elastic strain energy, energy released during propagation, plastic work stored, kinetic energy within the specimen during cracking and any work done against friction that opposes the movement of the tool over the crack faces.

$$F\,\mathrm{d}\delta = dU + G_c\,\mathrm{d}A + \mathrm{d}\Gamma + dKin + \mathrm{d}(friction) \qquad (2)$$

dU is the elastic strain energy which is shown in a general form and can be used for linear or non-linear cracked bodies. $G_c\, dA$ is the incremental work of crack propagation. $d\Gamma$ denotes the plastic work. $dKin$ refers to kinetic energy in the system and $d(friction)$ is the work done by friction during the forward movement of tool. In our studies we are dealing with a brittle, restrained rock specimen under quasi-static loading, hence the effect of plastic work and kinetic energy is neglected. Friction between the material and tool is generally modeled using Coulomb's relation of friction along surface but for this research we have not considered the effect of friction for simplicity.

3 PHASE FIELD APPROACH

3.1 Background

Problems involving fracture are of discontinuous nature. Models which represent cracks as such, are commonly known as discrete crack models. Several methods such as extended finite element method and cohesive zone element methods inculcate this discontinuity in the primary variable itself (e.g. displacement). The emphasis of these methods is on following the crack during the simulation. They generally rely on mesh enrichment or remeshing algorithms for this purpose. This is especially tedious when the crack geometry is delicate, and the propagation involves effects like branching and kinking. They also need an a-priori knowledge of the crack path. To surmount this problem a new technique based on minimization of energy has been prevalent in recent years to simulate crack growth in complex fracture networks. Unlike commonly used methods which rely on describing the cracks in a discrete manner, phase-field method describes the crack front related discontinuities in a smooth regularized sense. A Mumford-Shah functional (Mumford and Shah, 1989) is used to replace the crack surface by a smooth function. The variational problem thus formed when solved converges to the solution of sharp crack description in the Γ-convergence manner (Dal Maso, 1993). Fig (3) and (4) represent the difference between a sharp crack and the phase field model.

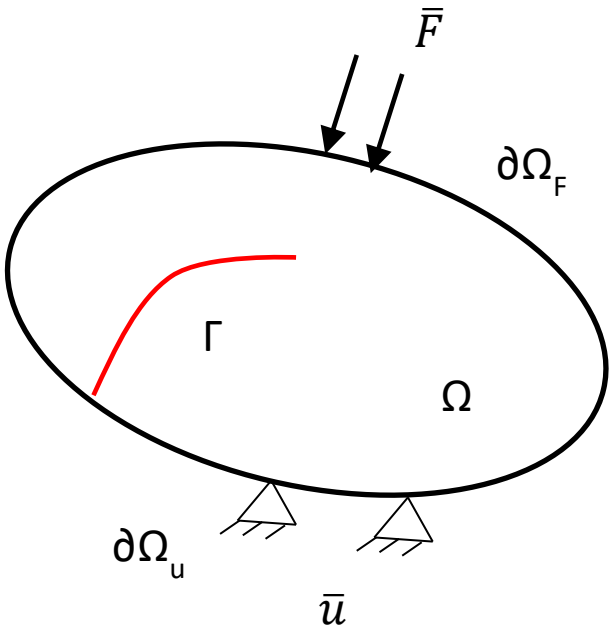

Figure 3: Sharp crack model

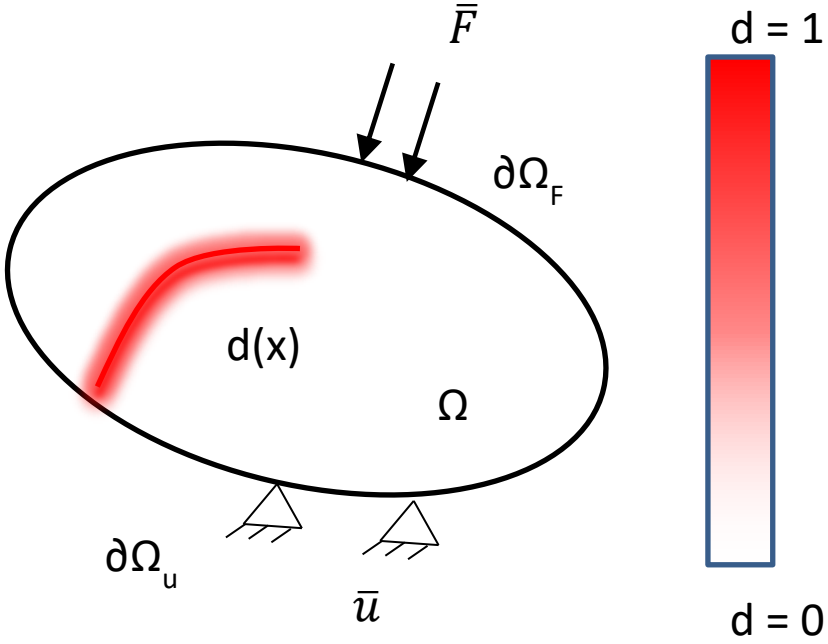

Figure 4: Regularized phase field depiction

In the phase field model, a new scalar field parameter is introduced with no discontinuity imparted in the displacement field. The process of fracture is represented by the evolution of this new parameter. This approximation which represents damage and undamaged states thus allows crack nucleation, branching and provides a scheme for crack propagation in general. The phase-field models can be regarded as gradient type damage model where the difference lies in choice of dissipation function and free energy. They primarily are two coupled non-linear system of partial differential equations (PDEs). One is the energy balance equation based on continuum mechanics and the other one is a PDE describing the phase field evolution. They can be solved in two ways, either using a monolithic scheme where the two equations are solved simultaneously to find solutions to the displacement and phase fields. Or a staggered scheme, which is an iterative approach where phase field is assumed constant to solve for displacement and then using the displacement, phase field is obtained. This is again repeatedly used to solve for displacement and continued until required accuracy is achieved.

One crucial characteristic of phase field models is the length scale parameter, ℓ. The transition width from undamaged state to completely damaged zone is controlled by this parameter. ℓ can also be construed as the regularized crack width. When length scale reaches the value of zero phase field models converge to Griffith's theory for brittle fracture. It seems alluring to use a very low value of ℓ, but in lieu of that an exceptionally fine spatial discretization would be needed, leading to excessively large stiffness matrices and hence more computational expense.

3.2 Phase Field and Gradient Damage Model

Let $\Omega \in \mathbb{R}^D$ be the configuration of a cracked solid with dimension D and $\partial\Omega$ being its boundary. In this regularized scheme crack geometry is represented by a smeared field defined by a scalar parameter d($\boldsymbol{x}$), $\boldsymbol{x} \in \Omega$, which takes a unit value on crack surface Γ and vanishes when away from it. Γ denotes a curve of dimension D – 1 within Ω (Refer Fig (3)). Miehe et al. (2010) show that this function can be obtained by using the minimization principle

$$d(\boldsymbol{x}) = Arg\left(\inf_{d \in S_d} \Gamma_l(d)\right) \tag{3}$$

subjected to Dirichlet-type boundary condition $S_d = \{d | \, d(\boldsymbol{x}) = 1 \; \forall \boldsymbol{x} \in \Gamma\}$

with

$$\Gamma_l(d) = \int_\Omega \gamma(d, \nabla d) \, d\Omega \tag{4}$$

representing the total crack length and

$$\gamma(d, \nabla d) = \frac{1}{2l} d^2 + \frac{1}{2} |\nabla d|^2 \tag{5}$$

denoting the crack surface density function per unit volume. The Euler equations of the variational principle (3) provides the subsequent boundary value problem on Ω:

$$\begin{aligned} & d - l^2 \Delta d = 0 \; in \; \Omega \\ & d(\boldsymbol{x}) = 1 \; on \; \Gamma \\ & \nabla d . \boldsymbol{n} = 0 \; on \; \partial\Omega \end{aligned} \tag{6}$$

where Δd is the Laplacian of the phase field and $\boldsymbol{n}$ the outward normal on the boundary $\partial\Omega$.

Length scale parameter l governs this regularization. Hence, $l \to 0$ annotates the topology of a sharp crack. This approximation can be easily visualised by Fig (5) and (6) which represents this regularization in a one-dimensional setting. Furthermore, Fig (6) shows the variation of diffusive crack topology over the one-dimensional domain of length L with respect to different widths of the length scale parameter.

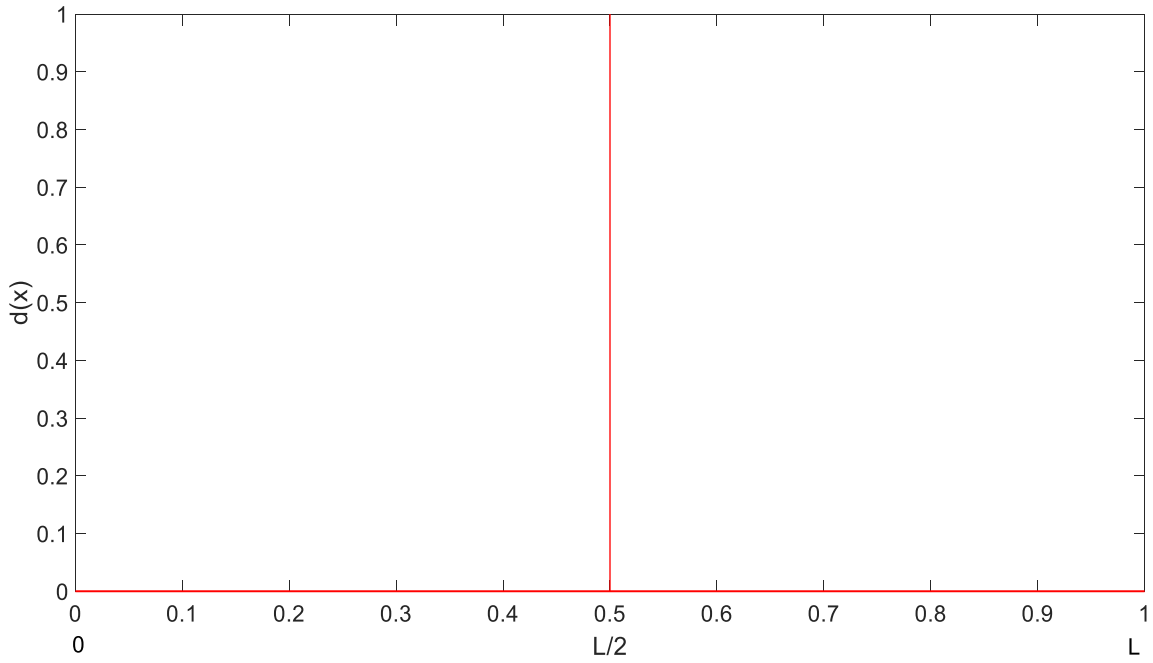

Figure 5: Sharp crack model with crack at x=L/2

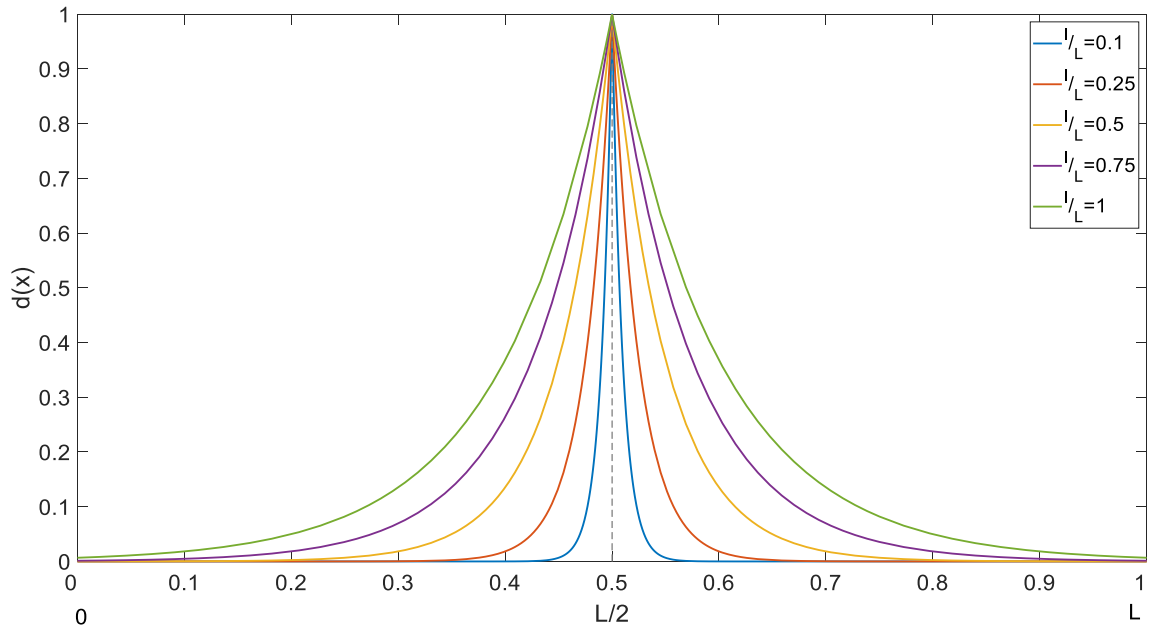

Figure 6: Diffusive crack representation with d =1 at x=L/2

3.3 Treatment of Length Scale as Material Property

The concept of intrinsic length scale has been a vital part of fracture mechanics since its introduction by Irwin (1958) who assumed that the plastic zone length in front of a propagating crack relates G_c to the material strength σ_c by

$$l_c = \frac{EG_c}{\sigma_c^2} \qquad (7)$$

Later Bazant and Cabot (1989) introduced a characteristic length describing the width of softening zone which corresponds to minimum spacing of cracks in discrete crack model and is given by

$$\ell = \alpha \frac{EG_c}{\sigma_c^2} \qquad (8)$$

with α being a non-local formulation parameter. The difference between these are that while l_c can be readily considered as a material parameter, ℓ due to its dependency on α is still a model parameter. The premises of this contrast have been discussed by Sargado et al. (2018) and Klinsmann et al. (2015) who argue that since the value of α is already known in case of a specific model, ℓ again acts as a material parameter depending on the other properties. Nguyen et al. (2015) also drew a comparison with phase-field regularization parameter l and showed with the help of experimental validation that l does depend on material parameters. They came up with the following relation for tensile test

$$l = \frac{27EG_c}{256\sigma_c^2} \quad (9)$$

3.4 Governing Equation and Numerical Implementation

3.4.1 Energy Aspects and Phase Field Problem

The origin of phase field formulation can be traced back to the fracture mechanics approach used by Francfort and Marigo (1998) which describes the energy functional as:

$$\mathrm{E}(\mathbf{u}, \Gamma) = \int_{\Omega \setminus \Gamma} \mathrm{W_u}(\boldsymbol{\varepsilon}(\mathbf{u}))\, \mathrm{d}\Omega + \mathrm{G_c H}_d{}^{D-1}(\Gamma) \quad (10)$$

where $\boldsymbol{\varepsilon} = \frac{1}{2}(\nabla\mathbf{u} + \nabla\mathbf{u}^{\mathrm{T}})$ is the strain field and $\mathrm{H}_d{}^{D-1}(\Gamma)$ denotes the Hausdorff surface measure associated with Γ. It symbolises the crack length or crack surface, depending on dimension (D) of the problem. The first term signifies the elastic energy stored in the body and the second term represents the energy used to create the crack based on Griffith criterion. The global minimization of this functional subjected to the irreversibility condition (Eq. (11)) can provide solutions for the unspecified displacements.

$$\Gamma_{t+\Delta t} \supseteq \Gamma_t \quad (11)$$

This condition ensures a continuous increase in crack length.

In a regularized framework one important alteration is replacing $H_d{}^{D-1}$ with an elliptical function that calculates the joint crack length. The energy functional for a cracked body thus becomes

$$E(\mathbf{u}, d) = \int_\Omega W_u(\mathbf{u}, d)\, d\Omega + G_c \int_\Omega \gamma(d)\, d\Omega \quad (12)$$

where, W_u is the energy density function, $\mathbf{u}$ is the displacement field, G_c is the energy release rate which is related to the fracture toughness K_I and $\gamma(d)$ is defined by Eq. (5). Following Miehe and Lambrecht (2001) which assumes isotropic behavior and accounts for damage caused by traction, the following form of W_u is considered

$$W_u(\mathbf{u}, d) = \psi^+(\boldsymbol{\varepsilon}(\mathbf{u}))\{g(d) + k\} + \psi^-(\varepsilon(\mathbf{u})) \quad (13)$$

The strain field $\boldsymbol{\varepsilon}(\mathbf{u})$ is further decomposed into tensile and compressive modes as

$$\boldsymbol{\varepsilon} = \boldsymbol{\varepsilon}^+ + \boldsymbol{\varepsilon}^-$$

and

$$\psi^+(\boldsymbol{\varepsilon}) = \frac{\lambda}{2}(\langle \mathrm{Tr}(\boldsymbol{\varepsilon})\rangle_+)^2 + \mu\, \mathrm{Tr}\{(\boldsymbol{\varepsilon}^+)^2\}, \quad (14)$$

$$\psi^-(\boldsymbol{\varepsilon}) = \frac{\lambda}{2}(\langle \mathrm{Tr}(\boldsymbol{\varepsilon})\rangle_-)^2 + \mu\, \mathrm{Tr}\{(\boldsymbol{\varepsilon}^-)^2\} \quad (15)$$

with

$$\boldsymbol{\varepsilon}^+ = \sum_{i=1}^{D} \langle \varepsilon^i \rangle_+ \mathbf{n}^i \otimes \mathbf{n}^i,\ \boldsymbol{\varepsilon}^- = \sum_{i=1}^{D} \langle \varepsilon^i \rangle_- \mathbf{n}^i \otimes \mathbf{n}^i$$

where ε^i and $\mathbf{n}^i$ are the eigenvalues and eigenvectors of $\boldsymbol{\varepsilon}$**.** The parameter $k \ll 1$ maintains the well-posed nature of the system for partially damaged domain. In the situation when $d \to 1$, k warrants the positivity of bulk energy. $g(d)$ is the stress degradation function

that reduces the material stiffness corresponding to the value of d. It is chosen in a way that the following conditions are satisfied:

i. $\mathrm{g}(0) = 1$, showing the material is initially undamaged,

ii. $\mathrm{g}(1) = 0$, indicating a fully damaged state,

iii. $\mathrm{g}'(1) = 0$, if the damage reaches a fully broken state this constraint safeguards the finite convergence of fracture force and

iv. $\mathrm{g}'(0) < 0$, enforcing that initially all the material points are intact.

The degradation function can be used in two ways to reduce the elastic strain energy density. One way is to multiply the entire energy with $\mathrm{g}(\mathrm{d})$, especially in isotropic formulation. The other way is to degrade the tensile part obtained by the decomposed compressive and tensile split of strain energy density as mentioned in Eq. (13).

The most common function that satisfies all the above conditions is the quadratic degradation function $\mathrm{g}_2(\mathrm{d}) = (1-d)^2$. This has been used in numerous finite element simulations pertaining to its simplicity and linear first derivative. An important observation with the use of this degradation function is that response in the regularized model unavoidably meanders from linear elastic nature before fracture. This deviation from linear elasticity with increasing displacement leads to a discrepancy in approximate and exact bulk energies. Some control over this incremental error can be achieved by careful formation of either the functional in-charge of crack length or the degradation function or both. Sargado et. al (2018) demonstrates a remedy to this by introducing a

family of exponential degradation functions which is talked about in section 3.4.3 of this thesis.

The inclusion of non-reversibility condition for phase field is a little complicated. This stems from the fact that the intermediate state of d lying between 0 and 1 does not have a clear physical meaning. The likely condition from a damage mechanics standpoint would be:

$$d(\boldsymbol{x})_{t+\Delta t} \geq d(x)_t \quad \forall\, x \in \Omega \tag{16}$$

To impose this Miehe et al. (2010) introduced a strain history functional

$$\mathrm{H}(\mathbf{x},\mathrm{t}) = \max_{\tau\in(0,\mathrm{t})}\{\Psi^{+}(\mathbf{x},\tau)\} \tag{17}$$

The following phase field problem is obtained by using the rate of energy functional and replacing the quantity ψ^{+} with H

$$\begin{cases} \mathrm{g}'(\mathrm{d})\mathrm{H} - \frac{\mathrm{G_c}}{l}\{\mathrm{d} - l^2\Delta\mathrm{d}\} = 0 & \text{in } \Omega \\ \mathrm{d}(\mathbf{x}) = 1 & \text{on } \Gamma \\ \nabla\,\mathrm{d}(\mathbf{x}).\mathbf{n} = 0 & \text{on } \partial\Omega \end{cases} \tag{18}$$

The weak form for phase field can be generated using the above equations. Taking the variation of d over the volume we have:

$$\int_{\Omega}\left\{\mathrm{g}'(\mathrm{d})\mathrm{H}\delta\mathrm{d} - \frac{\mathrm{G_c}}{l}(\mathrm{d} - l^2\Delta\mathrm{d})\delta\mathrm{d}\right\}\mathrm{d}\Omega = 0 \tag{19}$$

which can be written as the following using Gauss-Green theorem:

$$\int_{\Omega}\left\{\mathrm{g}'(\mathrm{d})\mathrm{H} - \frac{\mathrm{G_c d}}{l}\right\}\delta\mathrm{d}\,\mathrm{d}\Omega - \int_{\Omega}\mathrm{G_c}\,l\nabla\mathrm{d}\cdot\nabla(\delta\mathrm{d})\,\mathrm{d}\Omega + \int_{\mathrm{d}\Omega}\mathrm{G_C}\,l\nabla\mathrm{d}\cdot\mathbf{n}\delta\mathrm{d}\,\mathrm{d}\Gamma = 0 \tag{20}$$

The third term vanishes owing to the forced boundary condition and we are left with:

$$\int_{\Omega} \left\{ \left\{ \mathrm{g}'(\mathrm{d})\mathrm{H} - \frac{\mathrm{G_c d}}{l} \right\} \delta \mathrm{d} - \mathrm{G_c} l \nabla \mathrm{d} \cdot \nabla(\delta \mathrm{d}) \right\} \mathrm{d}\Omega = 0 \qquad (21)$$

The stiffness matrices for phase field are generated using this relation and the computations are executed in a quasi-static condition where in each n[th] step H_n is calculated from the previous load step extending Eq. (17) as:

$$H_n(\boldsymbol{x}) = \psi_n^+(\boldsymbol{x}) \qquad if\ \psi_n^+(\boldsymbol{x}) > \psi_{n-1}^+(\boldsymbol{x})$$

$$H_n(\boldsymbol{x}) = \psi_{n-1}^+(\boldsymbol{x}) \qquad if\ \psi_n^+(\boldsymbol{x}) \leq \psi_{n-1}^+(x) \qquad (22)$$

3.4.2 Displacement Problem

The weak form for displacement problem can be obtained by solving

$$\boldsymbol{u}(\boldsymbol{x}) = Arg \left\{ \inf_{u \in S_u} (E(\boldsymbol{u}, d) - W_{ext}) \right\} \qquad (23)$$

where $S_u = \{\mathbf{u} | \mathbf{u}(\mathrm{x}) = \bar{\mathbf{u}}\ on\ \partial\Omega$ and $W_{ext} = \int_{\Omega} \mathbf{f}.\mathbf{u}\, d\Omega + \int_{\partial\Omega_F} \bar{\mathbf{F}}.\mathbf{u}\, d\Gamma$ with f and $\bar{\mathrm{F}}$ being body forces and boundary tractions respectively. The weak form comes out as

$$\int_{\Omega} \boldsymbol{\sigma} : \boldsymbol{\varepsilon}(\delta \boldsymbol{u})\, d\Omega = \int_{\Omega} \boldsymbol{f} \cdot \delta \boldsymbol{u}\ d\Omega + \int_{\partial\Omega_F} \overline{\boldsymbol{F}} \cdot \delta \boldsymbol{u}\, d\Gamma \qquad (24)$$

$\forall \delta \boldsymbol{u} \in H_0^1(\Omega)$

where

$$\boldsymbol{\sigma} = \partial_{\varepsilon} W_u = (g(d) + k)\{\lambda \langle \boldsymbol{Tr\varepsilon} \rangle_+ 1 + 2\mu \boldsymbol{\varepsilon}^+\} + \lambda \langle \boldsymbol{Tr\varepsilon} \rangle_- 1 + 2\mu \boldsymbol{\varepsilon}^- \qquad (25)$$

In this work, analytical 1D and 2D problems are considered. The 2D problem is solved using the split scheme algorithm as discussed by Molnar and Gravouil (2017) and Nguyen et al. (2015). Appendix 1 focusses on the FE discretization and solving algorithm for 2D problem.

3.4.3 Analytical Approach and Suitable Degradation Function

In order to better fit our experimental results from scratch test we need a suitable degradation function which we can further use to generate desired stress-strain curves. We consider the family of exponential degradation function developed by Sargado et al. (2018).

$$g(d,k,n,w) = \frac{(1-w)\cdot 1-e^{-k(1-d)^n}}{1-e^{-k}} + wf_c(d) \quad (26)$$

Where $k > 0, n \geq 2\ and\ w \in [0,1]$ are parameters which affect the function and f_c is a corrector term. For our case we will consider $w = 0$. Fig (7) and (8) shows how different parameters affect this exponential degradation function. In both figures, a comparison with quadratic degradation function is also included.

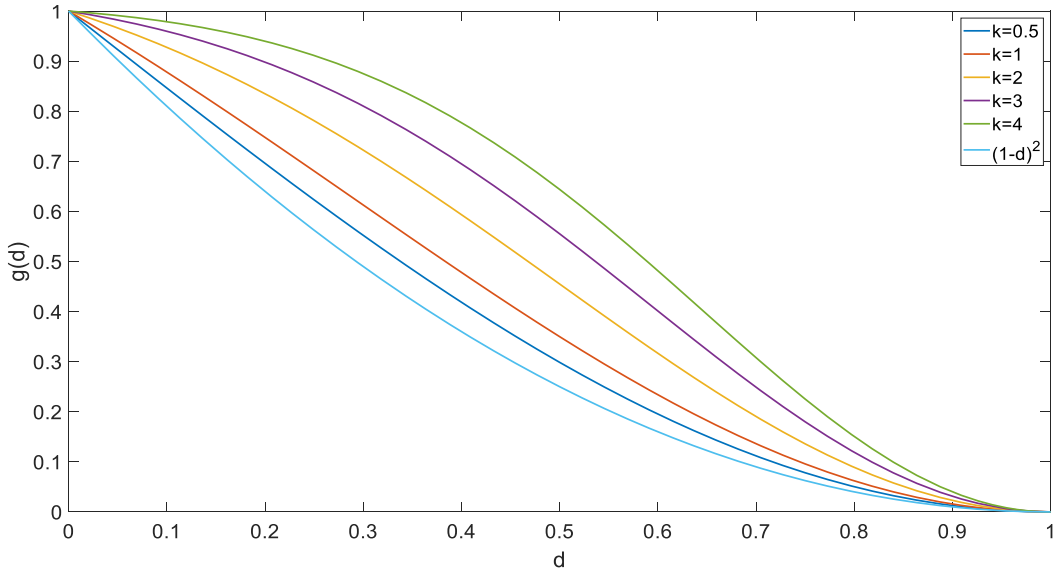

Figure 7: Variation of g(d) with parameter *k* (*n* assumed as 2)

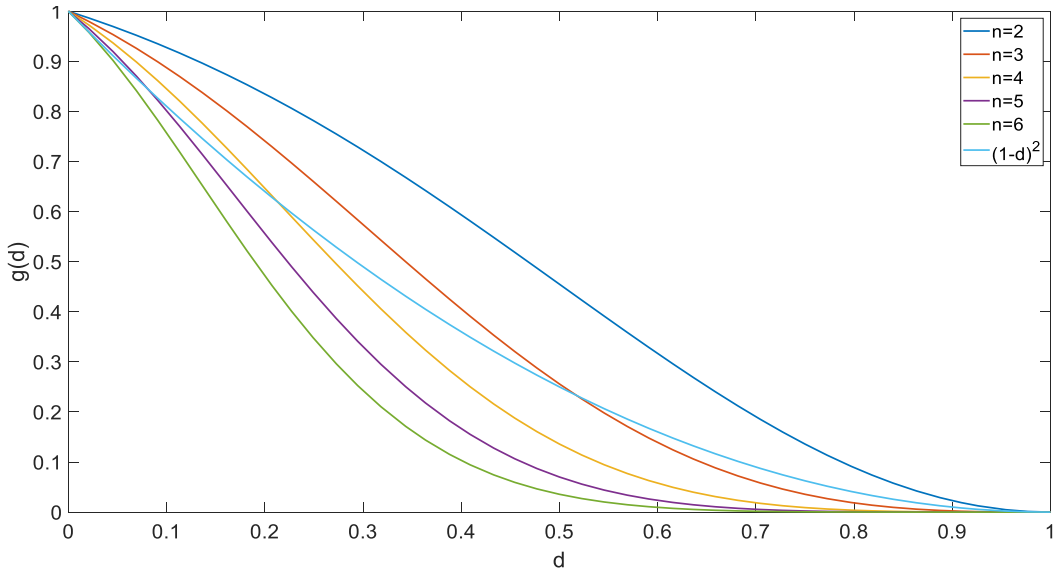

Figure 8: Variation of g(d) with parameter *n* (*k* assumed as 2)

To study the effects of these parameters we move forward by solving the governing equations (18) and (22) analytically for a 1-D problem. Considering a homogeneous bar of length 2L subjected to boundary conditions $u(\pm L) = \pm u_0$ and $d'(\pm L) = 0$ and having a uniform cross-sectional area as shown in Fig (9).

Figure 9: Boundary conditions for 1-D homogeneous bar under tension

Without body forces the equations for bar are reduced to

$$\frac{d}{dx}[\mathrm{g(d)s}(\varepsilon)] = 0 \qquad (27)$$

$$\mathrm{g'(d)}\psi - \frac{\mathrm{G_C}}{l}\left\{\mathrm{d} - l^2\frac{\mathrm{d^2(d)}}{\mathrm{dx^2}}\right\} = 0 \qquad (28)$$

where $\varepsilon = \frac{du}{dx}$, $s = E\varepsilon$ and $\psi = \frac{1}{2}E\varepsilon$. Assuming a spatial homogeneous phase-field i.e. $d(x) = d_0$. This means the stress is uniform as well giving $s = s_0 = E\varepsilon_0$. Using this assumption, the double derivative of phase field vanishes, and we can easily express ε as

$$\varepsilon(d) = \left[\frac{-2G_C d}{lE\mathrm{g'}(d)}\right]^{0\cdot5} \qquad (29)$$

The effective stress-strain curve which suffers damage because of presence of phase-field can be expressed as:

$$\frac{d[g(d)s]}{d\varepsilon} = \mathrm{g'}(d)E\varepsilon\frac{d(d)}{d\varepsilon} + \mathrm{g}(d)E \qquad (30)$$

Further manipulating and combining this with (21) we obtain the expression

$$\frac{\mathrm{d(g(d)s)}}{\mathrm{d}\varepsilon} = \frac{2\,\mathrm{d}[\mathrm{g'(d)}]^2 + \mathrm{g(d)}[\mathrm{g'(d)} - \mathrm{dg''(d)}]}{\mathrm{g'(d)} - \mathrm{dg''(d)}}E \qquad (31)$$

Now considering a limiting case of denominator of (23) going to zero an expression for k can be written as:

$$k(n) = \frac{(n-2)\,d^* + 1}{nd*(1-d^*)^n} \qquad (32)$$

where

$$d^* = \begin{cases} \frac{1}{3} & \text{if n} = 2 \\ \frac{(n+1)+\sqrt{5n^2-6n+1}}{2(n^2-2n)} & \text{otherwise} \end{cases} \qquad (33)$$

Plugging these in Eq. (25) and still using w as 0 gives us the degradation function with reduced parameters

$$g(d,n) = \frac{1-e^{-k(n)(1-d)^n}}{1-e^{-k(n)}} \qquad (34)$$

Using this in Eq. (30) we obtain the desired stress-strain curves which also depends on parameter n. Fig (10) shows the plot for dimensionless stress vs strain for several values of n.

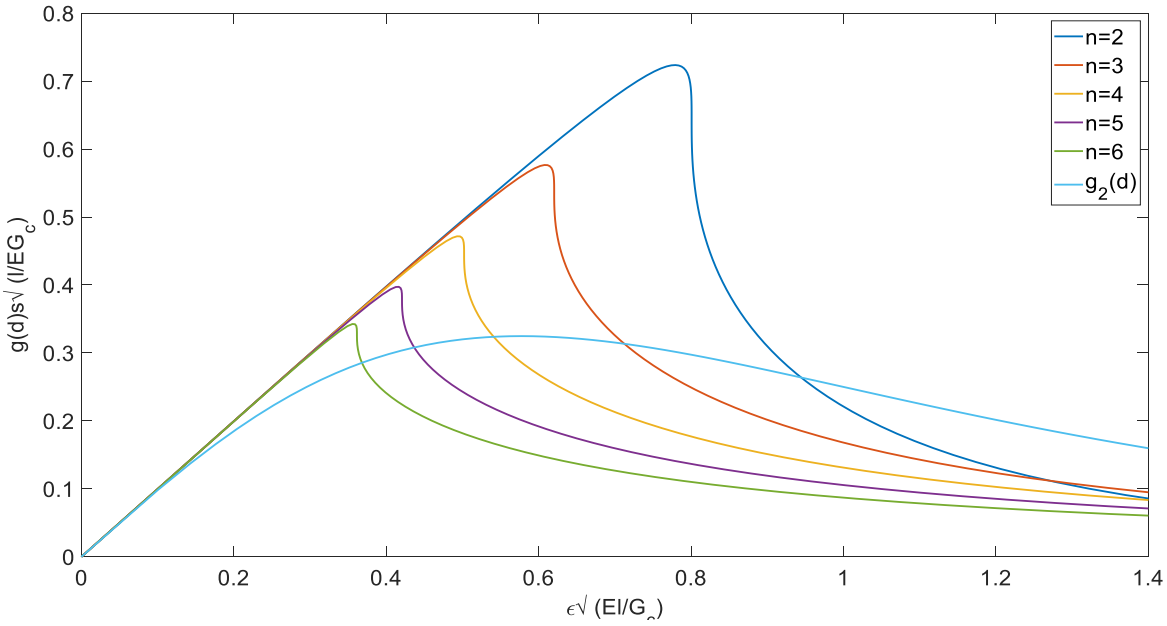

Figure 10: Stress-Strain curve for different degradation function

The above curve utilizes g(d) as a degradation function resulting from the phase field modelling of one-dimensional homogeneous bar in a tensile fracture setting. It suggests

the unique role that degradation functions play to generate the deviation from linear elastic behavior owing to the apparent propagation of crack. This is however manifested by the increase of damage i.e. the phase field parameter. Which then leads to higher degradation of stiffness and thus lower effective stress. Owing to this property, the above curve is chosen as the benchmark for evaluating internal energy density of the body.

4 EXPERIMENTAL CHARACTERIZATION

When talking about scratch test from a physical standpoint - its underlying mechanism during individual chipping occurrences is that the external work done by the tool will be converted into strain energy stored in the volume and the energy to create new surfaces. While approaching this problem from a phase field framework, the internal energy involves the damage induced to the material. In lieu of this, the above stress-strain curve in Fig (10) can be considered as a benchmark for calculating strain energy during the fracture process. Which is then compared to external work done derived from experimental data. We focus more on this relationship between the analytical and experimental aspects in the following sections.

4.1 Experimental Data and Setup

The experiment was performed on carbonate-rich shale sample (Eagle Ford shale). The fields of drilling and seismic exploration require an adequate knowledge of elasticity and strength among other properties of shales. But this prediction for organic rich scales due to their heterogeneous microstructure and complex chemical properties has always posed a significant challenge. Thus, researchers have kept producing innovative ways of combining experimental and theoretical aspects for a better understanding of this problem. The experimental data we have used is based on the study of outcrop organic rich and organic free Eagle Ford (found in west Texas) samples. The results of three tests were used to cover the experimental aspect. Table 1 shows the volume fraction of different material phases in the organic-free Eagle Ford sample.

Table 1: Volume fraction of distinct phases and porosity of organic-free eagle ford shale sample (Adapted from Mashhadian, Verde, et al., 2018)

Quartz (vol%)	Calcite (vol%)	Other (vol%)	Clay (vol%)	Porosity (%)
3	89	1	1	5.2

The data was collected by scratching the samples with a Rockwell diamond probe. This was done in both parallel and perpendicular to the bedding plane direction. In the experiment the indenter tool was moved through the surface of the material.

The tests were performed with a probe of radius 0.2 mm for scratch speed of 6 mm/min. The penetration depth was varied from surface to 0.1 mm. For a given test, horizontal and vertical force both were noted. Fig (11) shows the variation of horizontal force with scratch length in both parallel and perpendicular direction. This test was conducted three times in both the directions on the same material to arrive at a more detailed understanding.

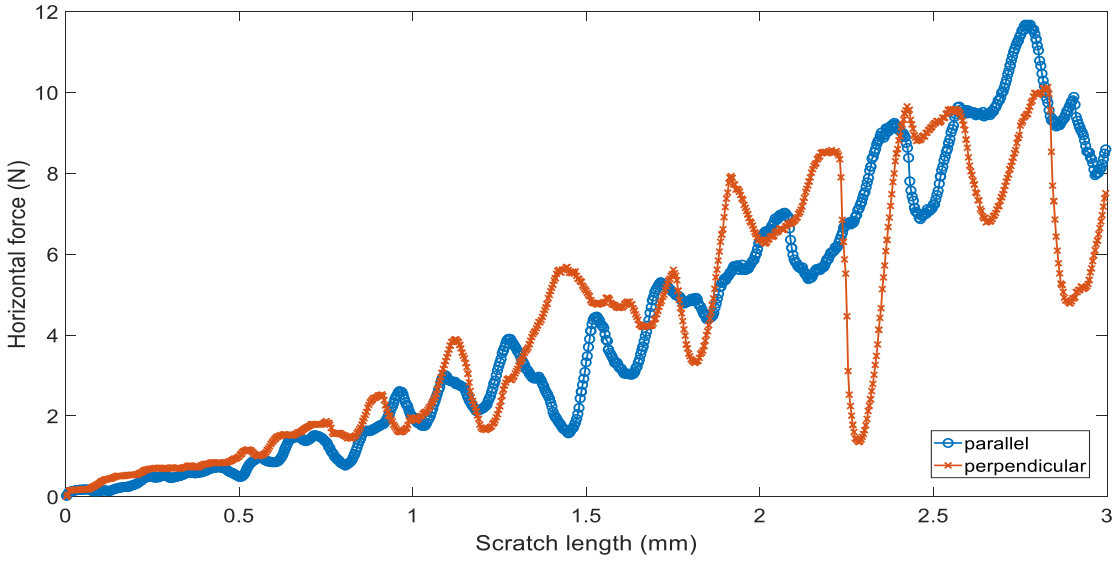

(a)

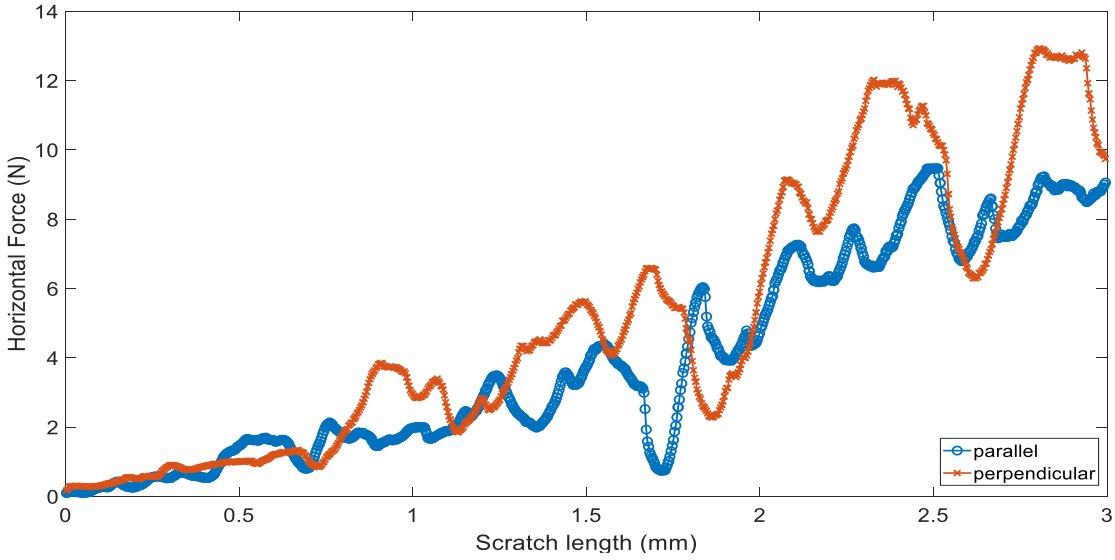

(b)

Figure 11:Scratch length vs horizontal force for the three experiments in both parallel and perpendicular direction; (a) Test 1, (b) Test 2, (c) Test 3

Figure 11 Continued

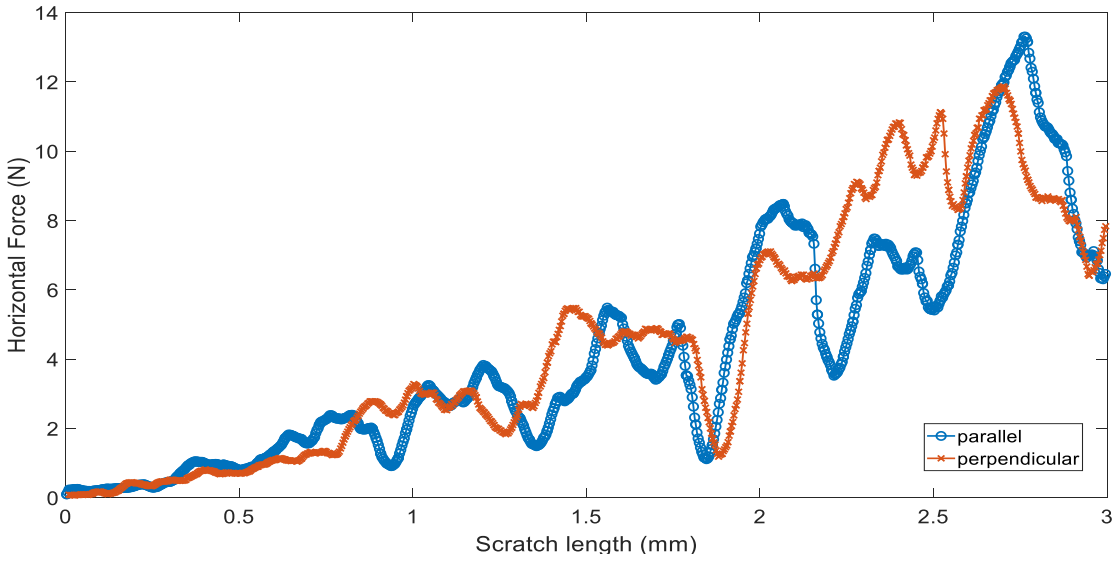

(c)

The violent drops in the horizontal force are quite understandable given the brittle nature of shale rock. Each peak represents the chipping phenomenon. The rate of change of vertical force however stays constant which gradually increases the penetration depth of the groove. Fig (12) shows the vertical force and depth changing with scratch length for the experiments in both parallel and perpendicular direction.

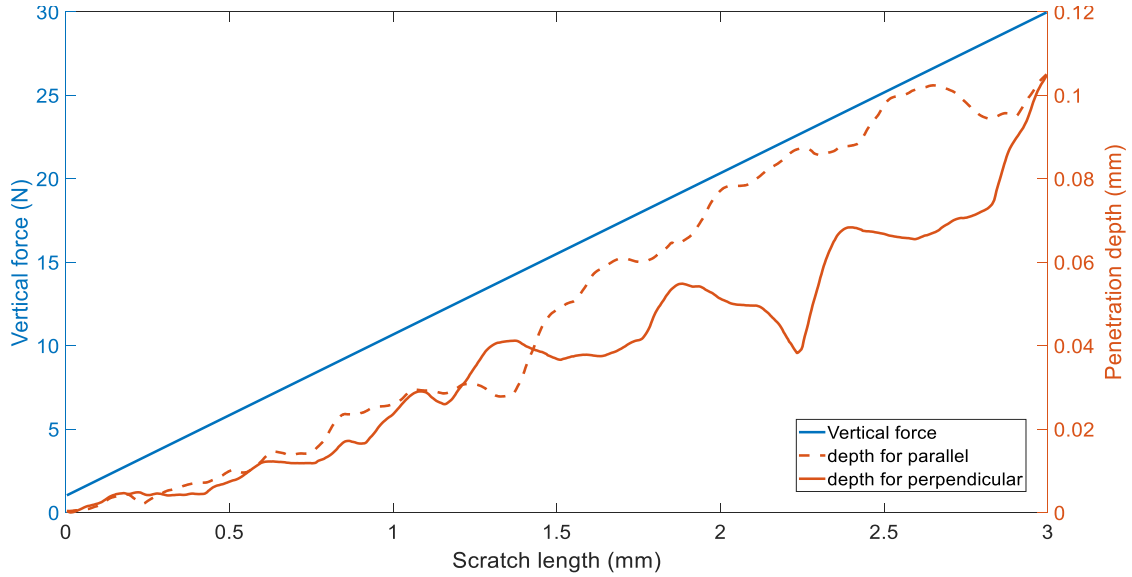

(a)

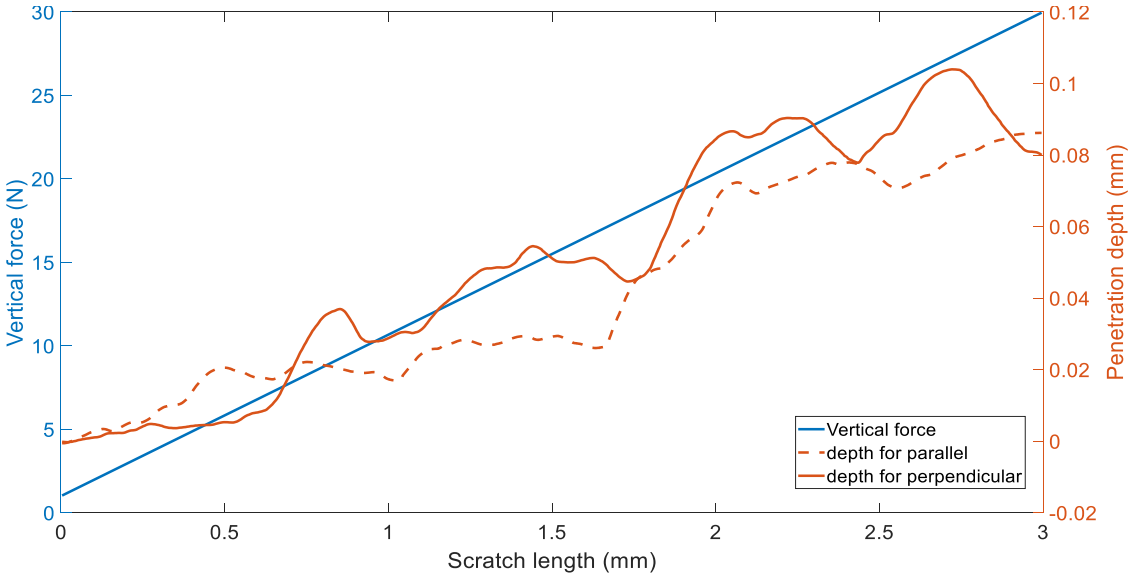

(b)

Figure 12: Scratch length vs vertical force and penetration depth for the three experiments in both parallel and perpendicular direction; (a) Test 1, (b) Test 2, (c) Test 3

Figure 12 Continued

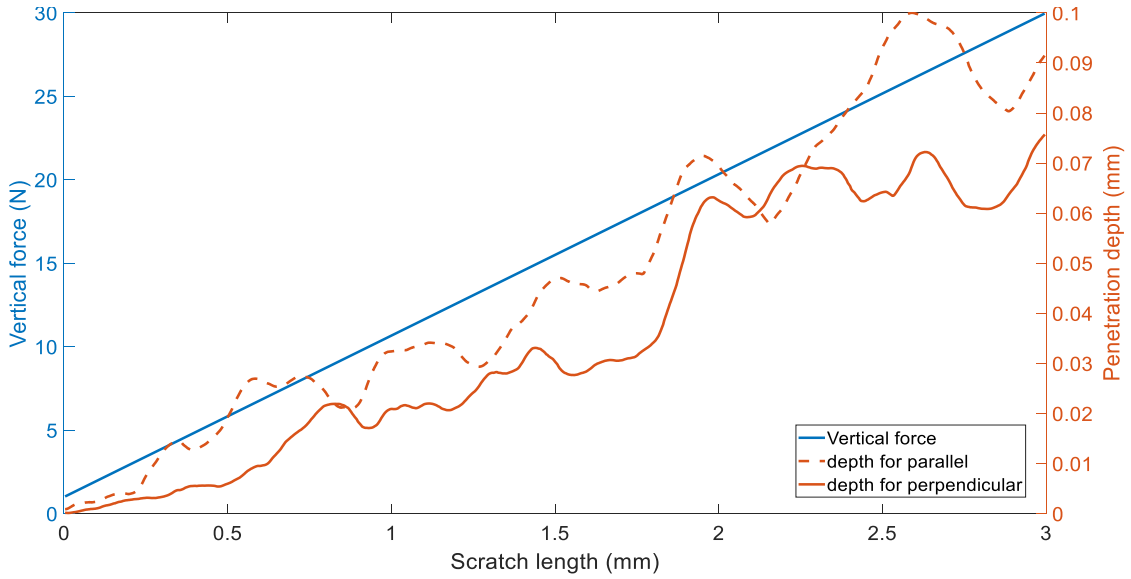

(c)

We focus on few of the well-formed peaks as shown in the scratch length vs horizontal force curves in Fig (11). Now, we can see from Fig (12) that the depth of cut changes during each individual chipping. But for simplicity we have assumed an average value of depth the tool moves during the offcuts.

4.2 Energy Equivalence and Length Scale Domain

As discussed in earlier sections when the tool moves forward, scratching the workpiece, it does an external work on the system. This external work (W_{ext}) contributes to the internal energy in the system and the energy released to create new surface. W_{ext} when normalised by per unit volume of the material chipped off produces external energy

density (U_{ext}). This can be obtained easily for each identified peak in the experimental data. On the other hand, the internal strain energy can be quantified by using a suitable material model for shale rock. This could be a model derived for either linear or non-linear cracked bodies. Then introducing the energy release rate (G_c) as a variable in the energy equation we could come up with an approximate value for G_c and then fracture toughness. However, if we use the phase field model as a method to approximate internal energy, we could directly utilize the stress-strain curve as a measure of strain energy density and energy released during crack propagation. Because the way phase field function is very similar to a damage framework. Since we are not dealing with a discrete crack in the model but a diffused one which is regulated by the damage parameter over a length scale. The advantage of using the dimensionless stress-strain curve obtained in section 3.4.3 is that we can keep the length scale l and G_c as a variable. They will later be used as a multiplier to reach at the strain energy density. The comparison of this to U_{ext} will give a straightforward equation but in two variables, namely l and G_c. Hence, in order to determine the span of fracture toughness, a range of values of l will be required. This in an indirect sense means that the length scale can be treated as an intrinsic material property. Several researchers have strived towards making this connection more profound. Detournay et al (2008) have talked about internal and characteristic length scales of the material to better understand the tool-rock interaction and the different modes of failure. In our research we have bounded the length scale corresponding to the mathematical phase field model between the following physical length scales:

- ℓ_m or material length scale

- ℓ_p or process length scale

Material length scale, which is correlated with flaw length, is also closely related to maximum grain size of rocks. However, it is also noteworthy to mention that based on the definition of phase field equations the length scale's lower bound can go to 0, which then would suggest a discrete crack model. The process length scale in terms of scratch test can be referred to the horizontal distance moved by the tool for indentation and depth of cut for cutting. We have considered the length scale to lie between the range of maximum grain size and depth of cut ($\ell_m < l < \ell_p$). Using this and the comparison of external and internal energies we have arrived at a range of values for fracture toughness for shale rock. The algorithm for this procedure is explained in Appendix B. In order to give more credibility to our analytical approach we have also performed 2D phase field finite element simulations of scratch test on a shale specimen and observed the chipping behaviour.

4.3 2D Finite Element Approach

The main purpose of this simulation is to validate the phase field model used for scratch test in a 2D space. The phase field and displacement problem were solved using shifted strain split algorithm to avoid the non-linearity related to decomposition of strain field. The details of algorithm and discretization and further derivations of stiffness

matrices are explained in Appendix 1. Two kinds of two-dimensional model were considered for this simulation:

i) An uncracked specimen – an initial crack surface was not modelled. The displacement increment was applied along the depth of cut to imitate the movement of tool and the results were recorded.

ii) A cracked specimen – An initial crack surface was modelled. As the tool scratches and moves into the material, compression crushing takes place at the interface. Due to this there is a possibility that crack has already initiated. To achieve this the displacement increment was applied along the depth of cut but with a crack surface modelled where the bottom of the tool must have been.

We considered a domain of side length L =1 mm with a notch of average depth c =0.07 mm at an angle of θ =15° cut away at the corner for the uncracked case. This depth is calculated based on observing the experimental data and taking the mean during one of the chipping events. The bottom end (y=0) of the domain was restricted along x and y directions. The left and right ends (x=0 and x=L) were blocked in x direction in order to replicate the scratching experiment. The angled notch accommodates the moving tool; hence a uniform x-displacement is applied over this area which is increased with time. Because of this a crack initiates and propagates imitating the chipping phenomenon. One complexity that arises in this case is how the vertically downward load is applied. This downward load during experimental scratch test guides the tool and is used to gradually

increase the depth. Fig (13.a) shows the geometry and boundary condition for the model.

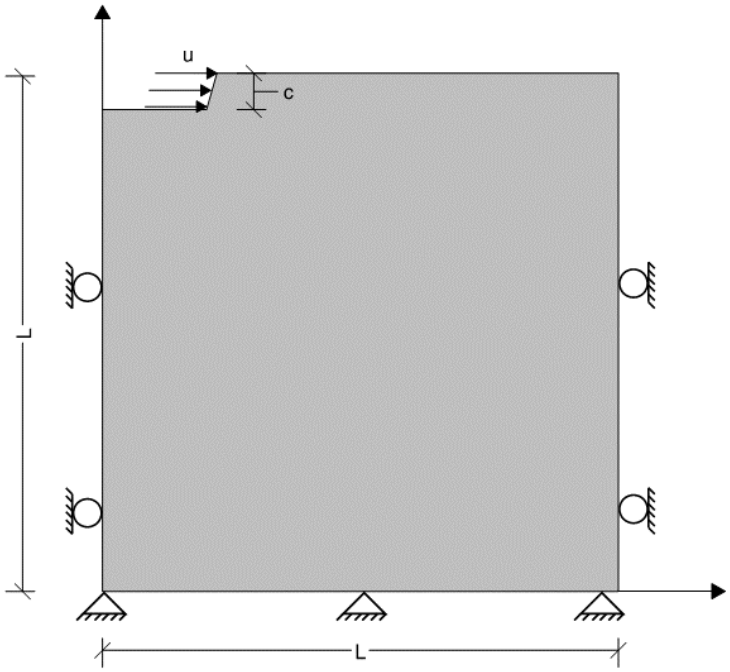

(a)

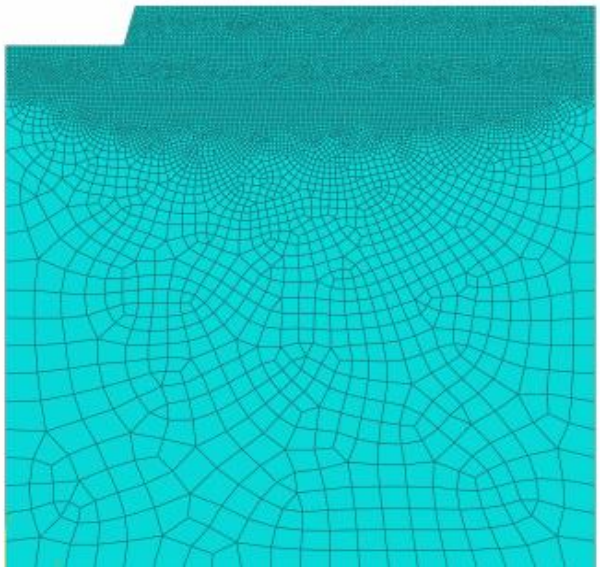

(b)

Figure 13: (a) Geometric setup and restraints for uncracked case; (b) FE mesh

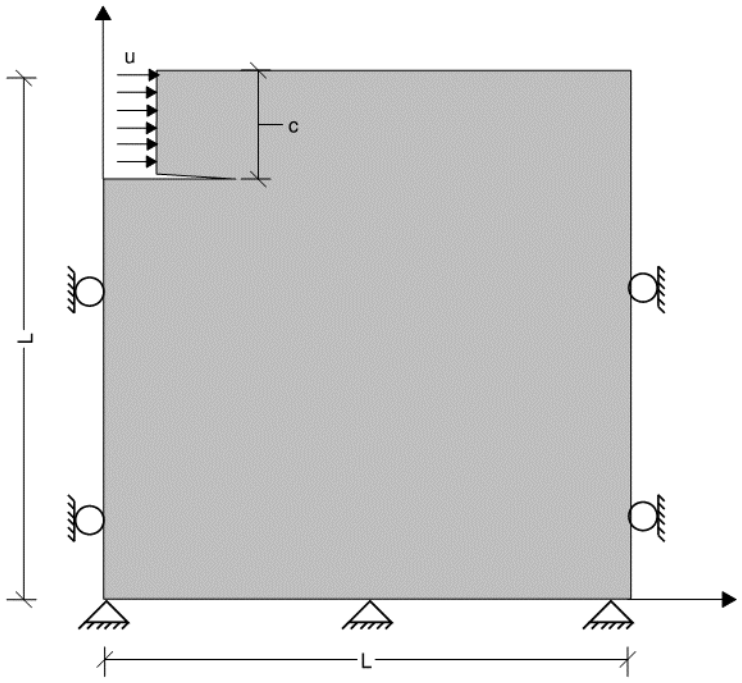

(a)

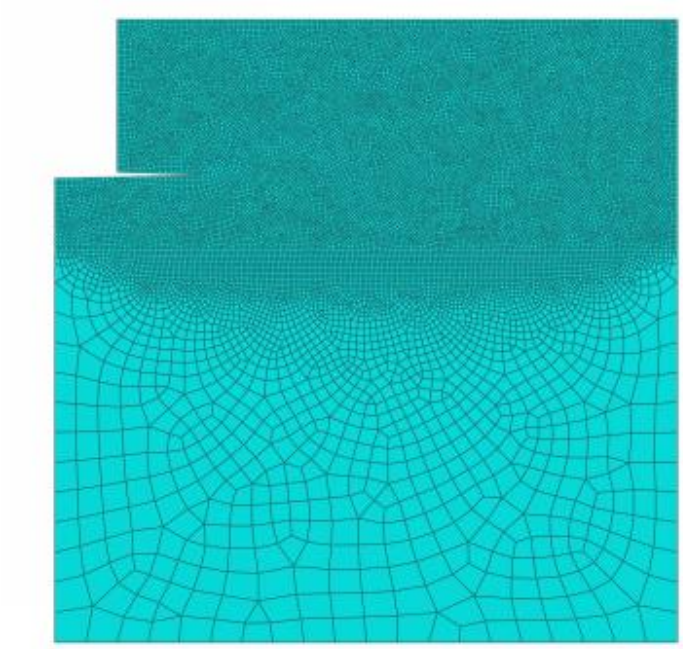

(b)

Figure 14: (a) Geometric setup and restraints for cracked case; (b) FE mesh

For the uncracked case, the domain is meshed according to the initial geometry and is refined in the zone where crack is expected to propagate as shown in Fig (13.b). The mesh consists of 10716 rectangular elements. In the second case, an initiated crack of 0.1 mm is also modeled (Fig (14)). The mesh comprises of 20796 elements. The typical size of the element in the propagation zone is kept at least half of the approximated length scale and a size of 0.05 mm is used in the remaining area of domain.

The state of plane strain is assumed. The modeled solid is assumed to be homogeneous isotropic with following properties: Young's modulus (E) = 70 GPa and fracture toughness of 1.4 MPa$\sqrt{m}$. The computation was carried out in a displacement-controlled context with fixed displacement increments of $u = 10^{-5}$, assessed with 1500 load increments.

5 RESULTS AND CONCLUSIONS

The comparison of internal and external energies led us to determine a range of values for fracture toughness of the shale rock specimen. 3 experiments were conducted in both the direction of bedding plane. Section 5.1 shows the obtained plots for the variation of fracture toughness with length scale bounds. In addition to this the results of 2D simulations in the form of phase field and displacement contours is shown in section 5.2.

5.1 Determination of Fracture Toughness

5.1.1 For Scratch Parallel to Bedding Plane

Every data point in Fig (15) represent a fracture toughness calculated for the range of length scale lying between material and process length scale. The considered Young's modulus in this direction is 70 GPa. A comparison is drawn to a prevalent value of fracture toughness in this direction of bedding plane. For the type of shale used, this value lies closer to 1.4 MPa$\sqrt{m}$. The mean relative uncertainty in the evident fracture toughness in this direction is 28%.

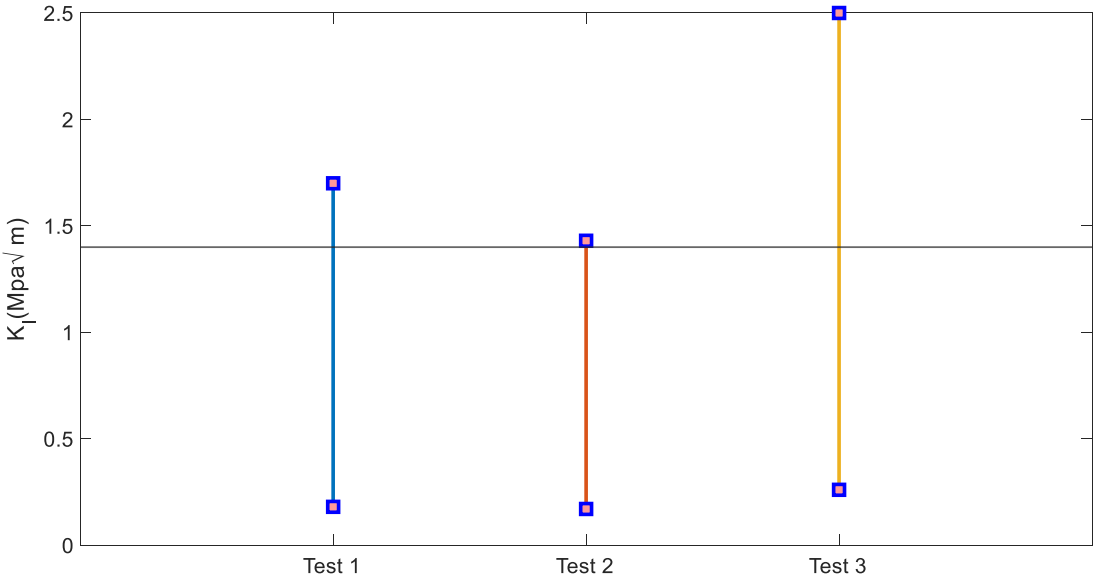

Figure 15: The range of fracture toughness in parallel direction within the bounds of length scale (ℓ_m<l<ℓ_p). Lower values of K_I correspond to ℓ_m and increase with increment in length scale

The study based on the effect of alternative degradation function is laid out in Fig (16). It can be concluded that the influence was not significant in the one-dimensional problem. This can be pertaining to the fact that we only used the stress-strain curve to calculate internal energy density and not individual peaks. The lower parameter degradation even though showed a higher peak (refer to Fig (10)), during the post peak behaviour it attained the state of full damage i.e. phase field reaching the value of 1 and effective stress reaching the value of 0, quicker than other degradation function. Thus, producing a similar area under curve.

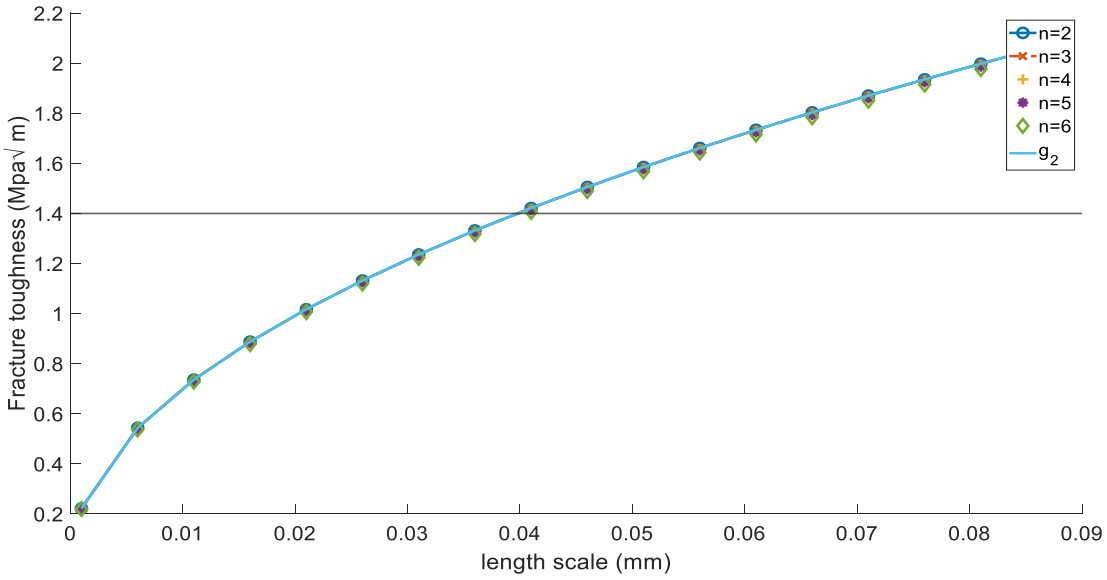

Figure 16: Variation of fracture toughness based on choice of degradation function

Fig (17) shows the fracture toughness calculated from the analytical model when the scratching is done parallel to bedding plane direction. Each peak refers to an increment in depth of cut and external energy evaluated using the horizontal force and tool-displacement in corresponding region. The observed value lies somewhere between 0.2-2 MPa√m.

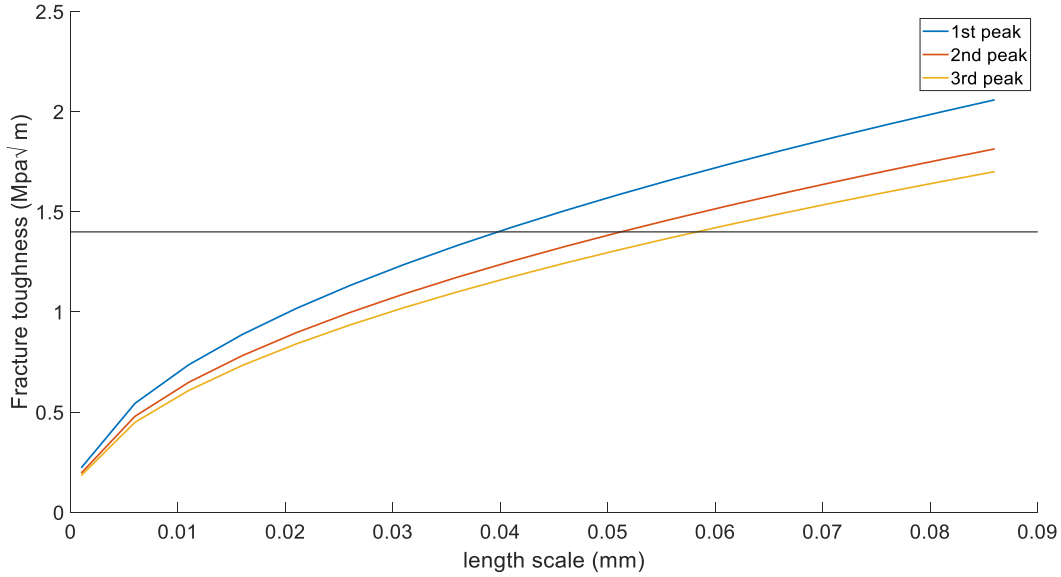

(a) Test 1

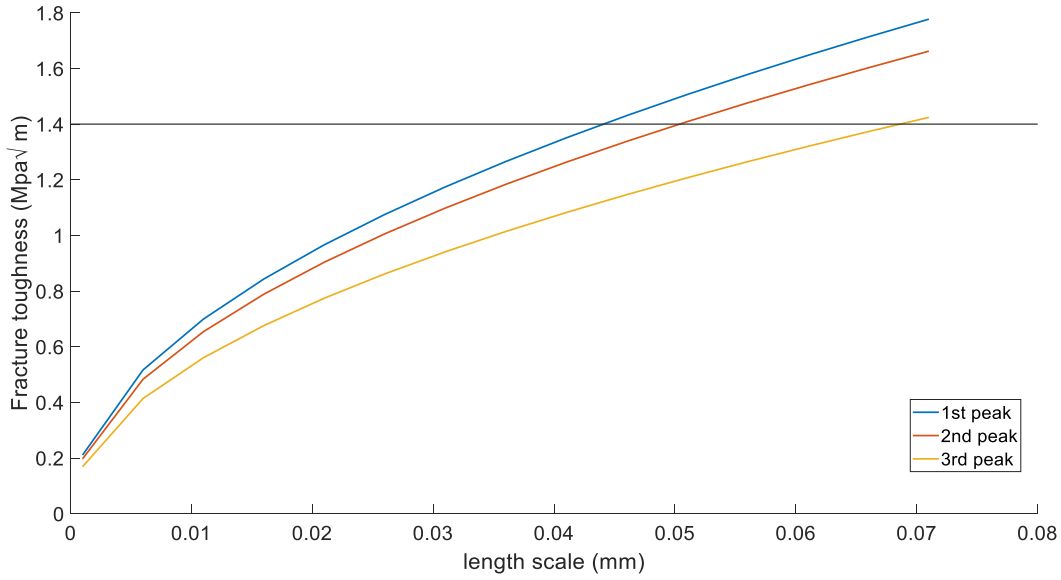

(b) Test 2

Figure 17 : Obtained fracture toughness variation with length scale for different chipping occurrences when scratched parallel to bedding plane direction; (a) Test 1, (b) Test 2, (c) Test 3

Figure 17 Continued

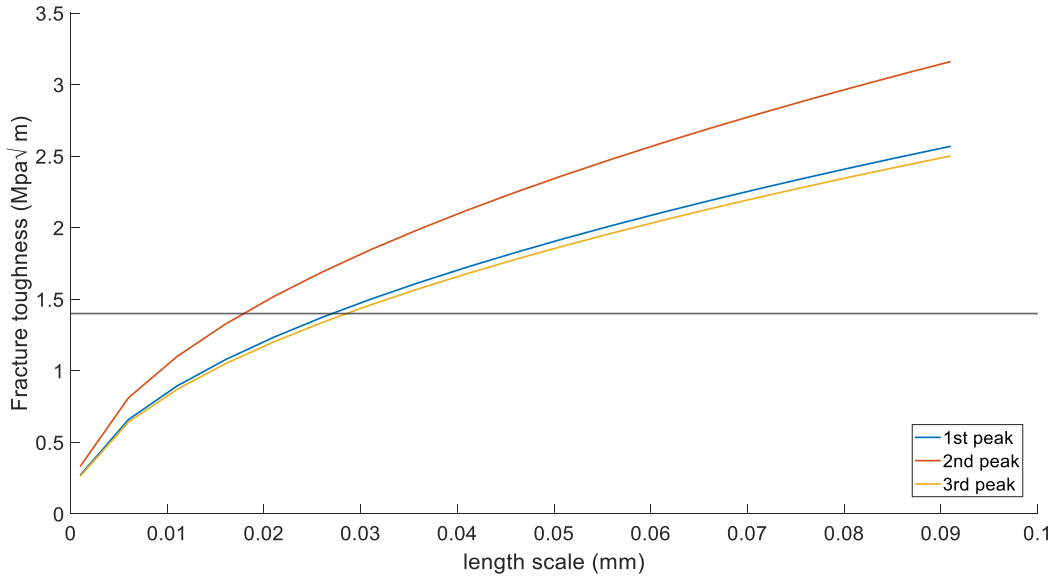

(c) Test3

5.1.2 For Scratch Perpendicular to Bedding Plane

This section is similar to the previous section with difference lying in the direction of scratching which leads to a clear difference in fracture properties. Fig (19) shows the fracture toughness calculated from the analytical model when the scratching is done perpendicular to bedding plane direction. The considered Young's modulus in this case is 210 GPa. For a given test, the fracture toughness lies along both the sides of the common value of 2.5 MPa√m. The mean relative uncertainty in the visible fracture toughness in this direction is 36%. It must not be overlooked that shale is vastly anisotropic and heterogeneous in nature. This is also evident from the variation obtained in fracture toughness in the same sample but at a greater depth.

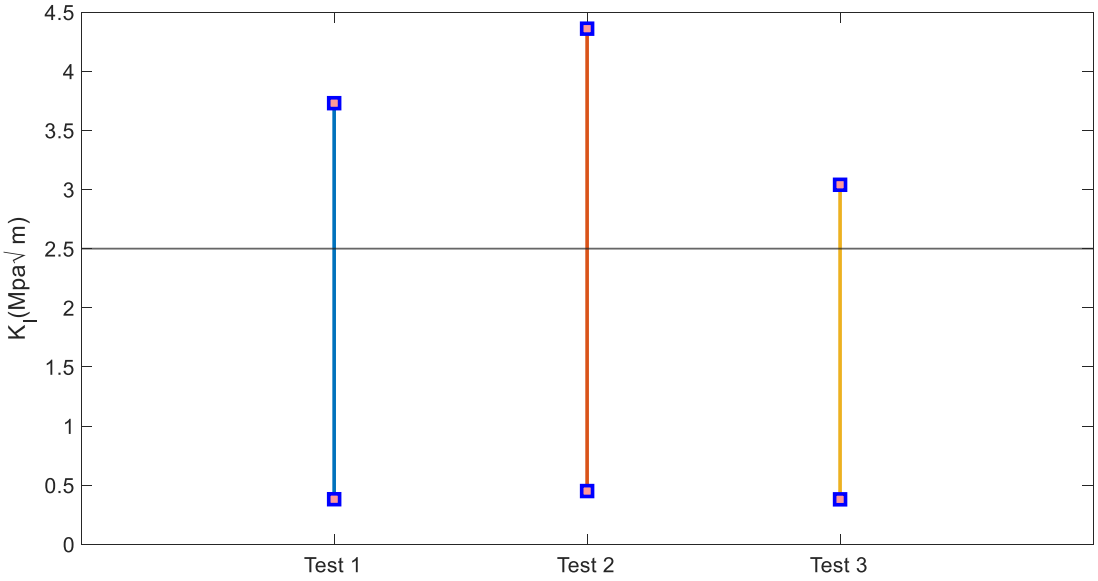

Figure 18: The range of fracture toughness in perpendicular direction within the bounds of length scale (ℓ_m<l<ℓ_p). Lower values of K_I correspond to ℓ_m and increase with increment in length scale

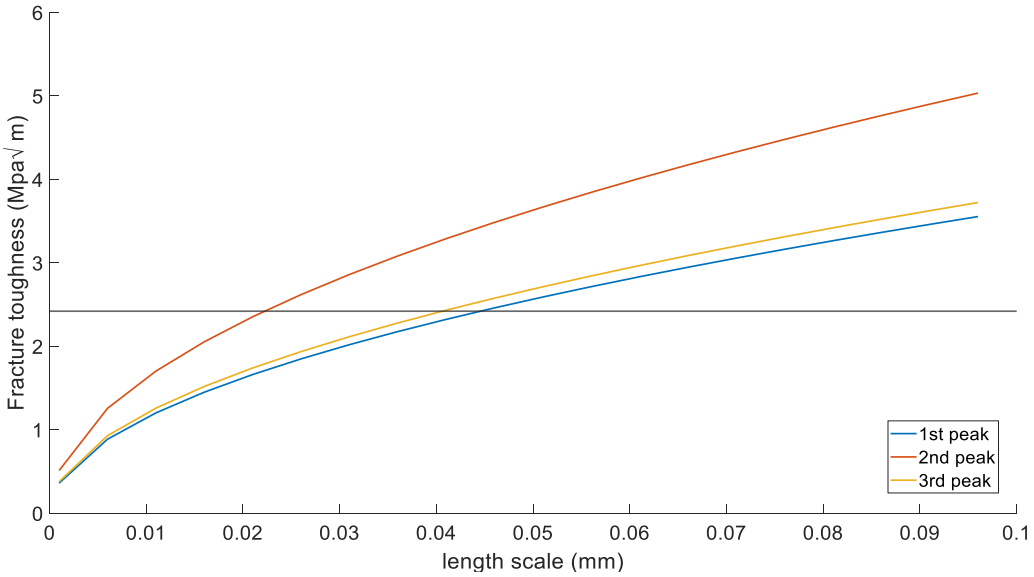

(a) Test1

Figure 19: Obtained fracture toughness variation with length scale for different chipping occurrences when scratched perpendicular to bedding plane direction; (a) Test 1, (b) Test 2, (c) Test 3

Figure 19 Continued

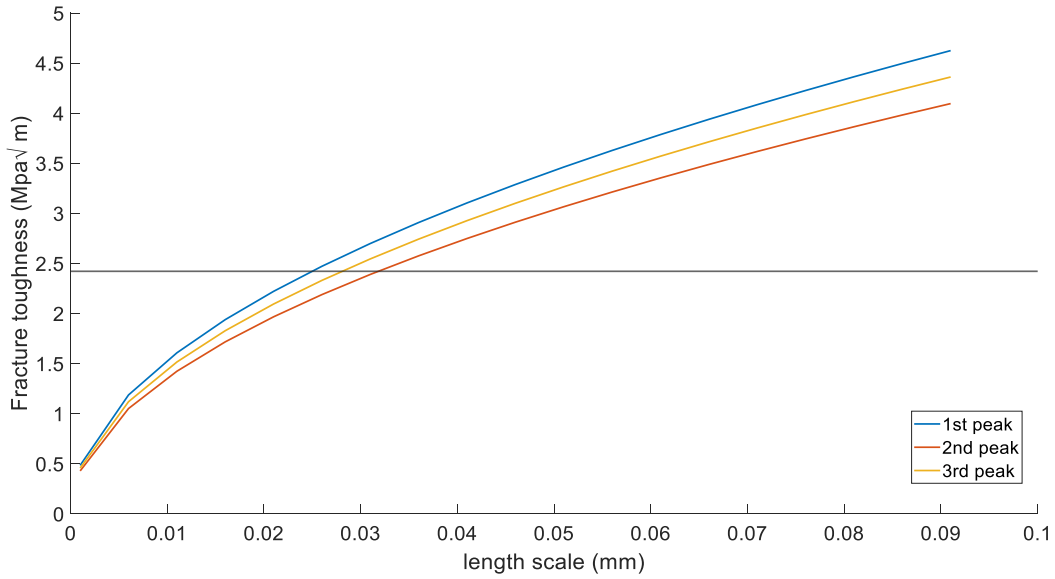

(b) Test2

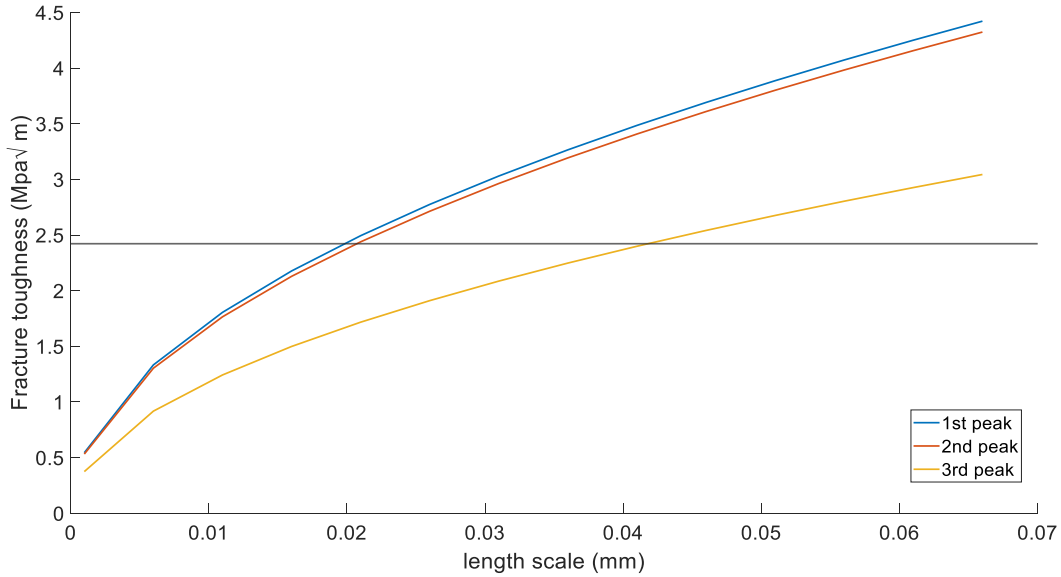

(c) Test3

5.1.3 Summary of Analytical Results

Table (2) summarizes the fracture toughness obtained in both parallel and perpendicular direction based on the bounds of material and process characteristic length.

Table 2: Summary of fracture toughness obtained from analytical phase field model

	parallel			**perpendicular**		
	characteristic length(mm)		G_c (MPa√m)	characteristic length(mm)		G_c (MPa√m)
Test1	ℓ_m	0.004	0.37	ℓ_m	0.004	0.76
	ℓ_p	0.087	1.70	ℓ_p	0.099	3.73
Test2	ℓ_m	0.004	0.34	ℓ_m	0.004	0.91
	ℓ_p	0.075	1.43	ℓ_p	0.094	4.36
Test3	ℓ_m	0.004	0.52	ℓ_m	0.004	0.75
	ℓ_p	0.092	2.50	ℓ_p	0.067	3.04

Although this comparison was based on a phase-field simplified analytical model with distributed damage in a tensile setting. This approximation can be supported by the fact that within the framework of strength of material, the onset of fracture is due to maximum tensile stress reaching the tensile strength of material, and that the tensile features at rock chip surface has been stipulated by field and experimental evidence (Richard 1999). A further comparison by a more detailed and realistic 2D computational model based on

phase field in the next section provide further insight regarding the validation of this simple analytical approach.

5.2 2D Simulation Verification

The numerical 2-D finite element model solving the phase field and displacement problem simultaneously is used to draw a contrast between the chipping length obtained from the model and experiment. The contour for phase field are plotted in this section. Wherever the values of damage parameter reached unity or closer shows the path the crack must have followed. Chipping length is calculated by measuring the path the crack traversed. Revisiting the results in section 5.1 for experiments done parallel to the bedding plane, it can be observed that a length scale value in the vicinity of 0.04 mm gives a fracture toughness value closer to 1.4 MPa$\sqrt{m}$. Pertaining to that a length scale of 0.04 was chosen for 2D simulation.

5.2.1 Scratching without Considering an Initial Crack Surface

Fig (20) shows the evolution of phase field as the displacement along the notch is increased. As there is no consideration of crack surface, the imitated tool movement presses against the notch, the diffused crack can be seen originating at the corner. And as it progresses the material ahead is degraded in its entirety.

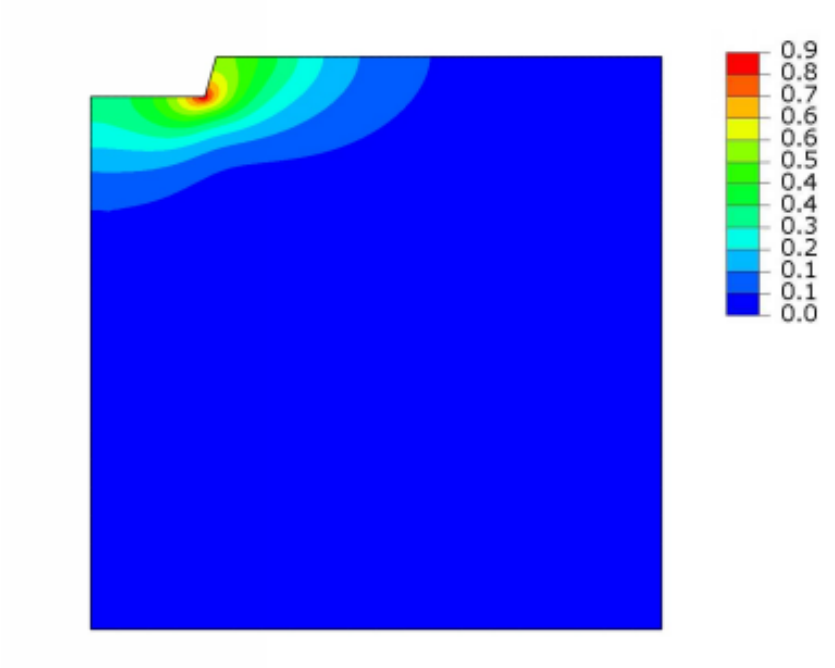

(a)

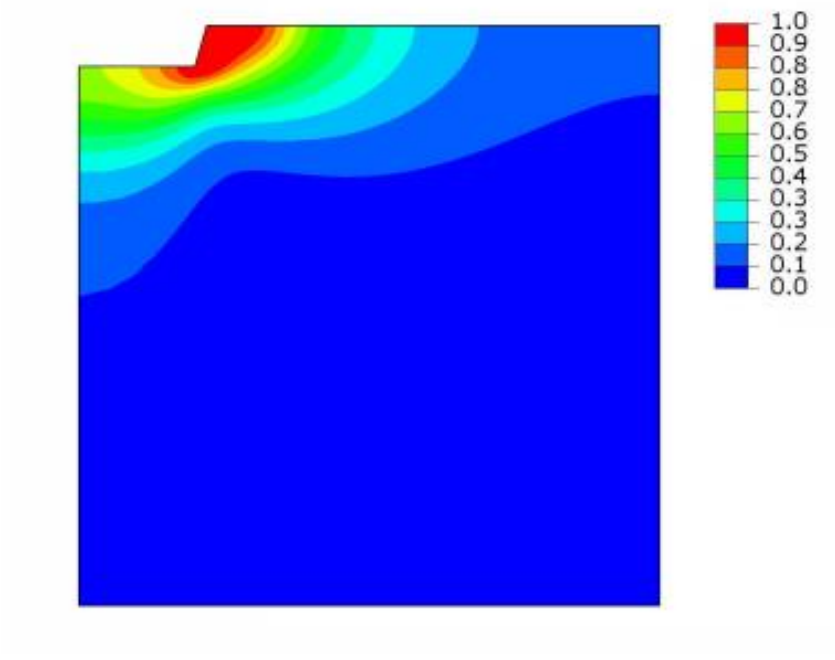

(b)

Figure 20:Phase field distribution at a) u = 5.10-4 mm; b) u = 2.10-3 mm

When the propagation completely reaches the free surface, that is where we know the chipping has occurred. A crucial observation here is the compression crushing happening in front of the tool. The chipping length obtained from 2D simulations came out to be 0.16 mm which is quite close to the observed value of 0.22 mm in the first experiment.

5.2.2 Scratching while Considering an Initial Crack Surface

For the case when a crack surface is modelled initially, the diffused crack propagates from the tip and moves towards the free surface. The path that it crosses can be interpreted as the chipping length. Fig (21) shows the evolution of phase field as the displacement along the notch is increased.

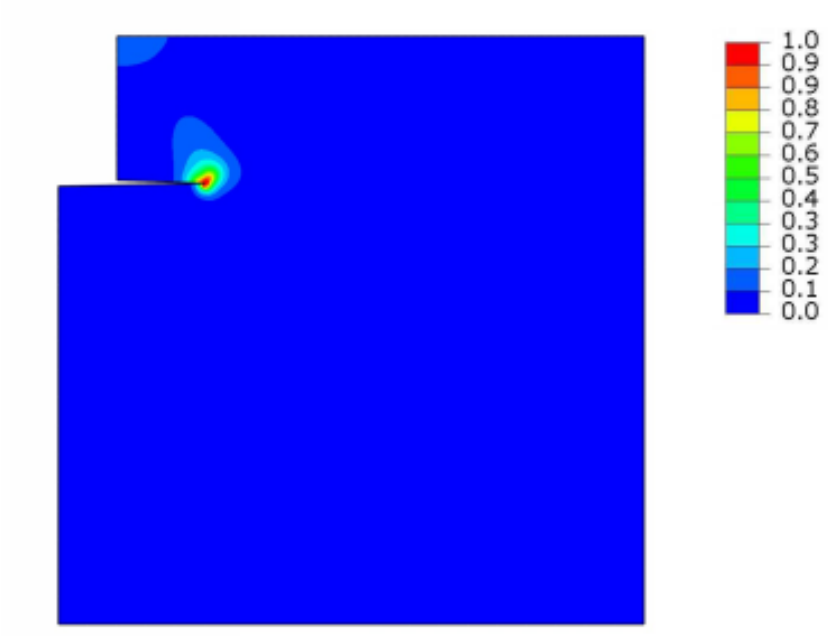

(a)

Figure 21: Phase field distribution in cracked specimen at a) u = 6.10-4 mm; b) u = 3.10-3 mm; c) u = 8.10-3 mm

Figure 21 Continued

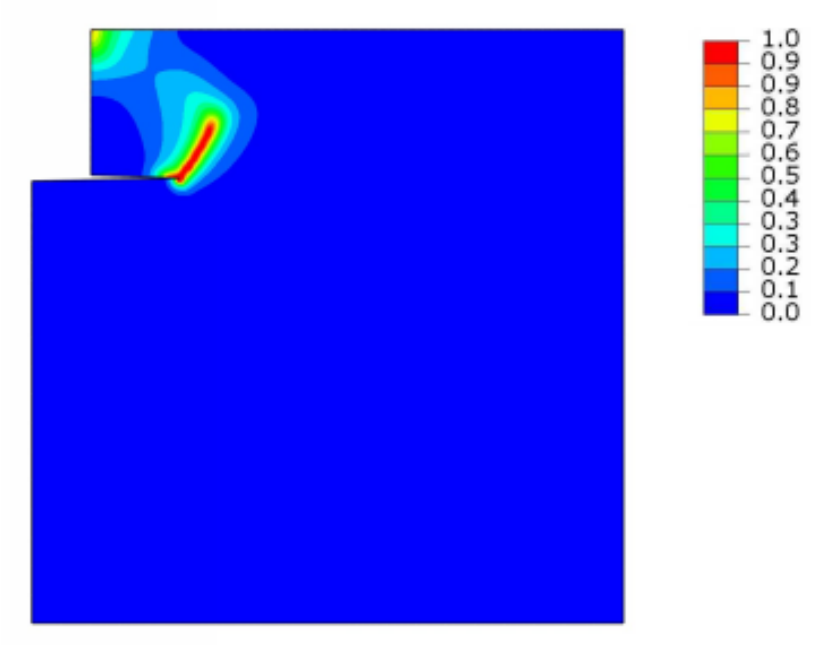

(b)

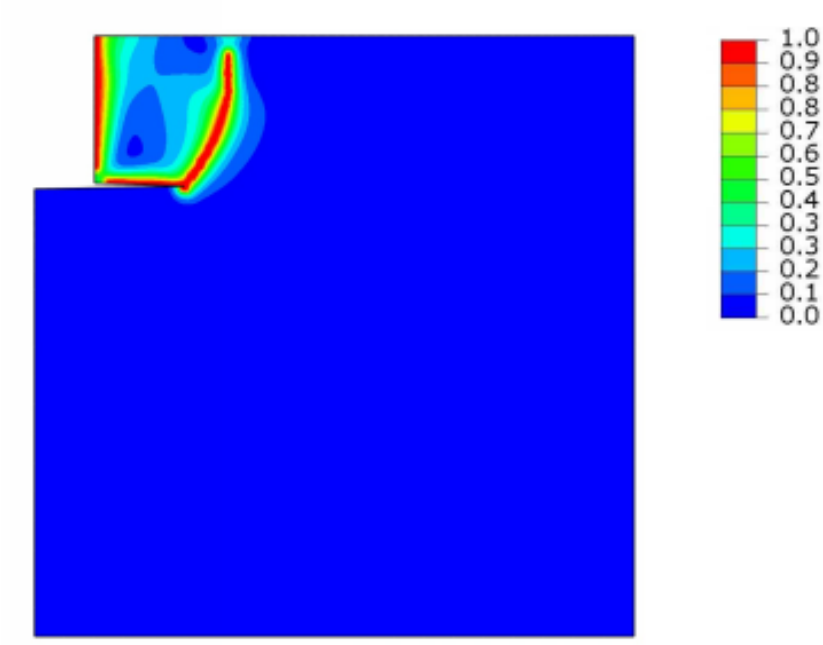

(c)

The chipping length obtained in this case is 0.23 mm. However, this includes the initial crack length. A critical observation in this scenario is in addition to the propagation of crack there is damaging of material where the force is applied. This is most likely due to the application of vertically downward load to better replicate the experimental scenario and the complexity arose when considering this as a boundary condition.

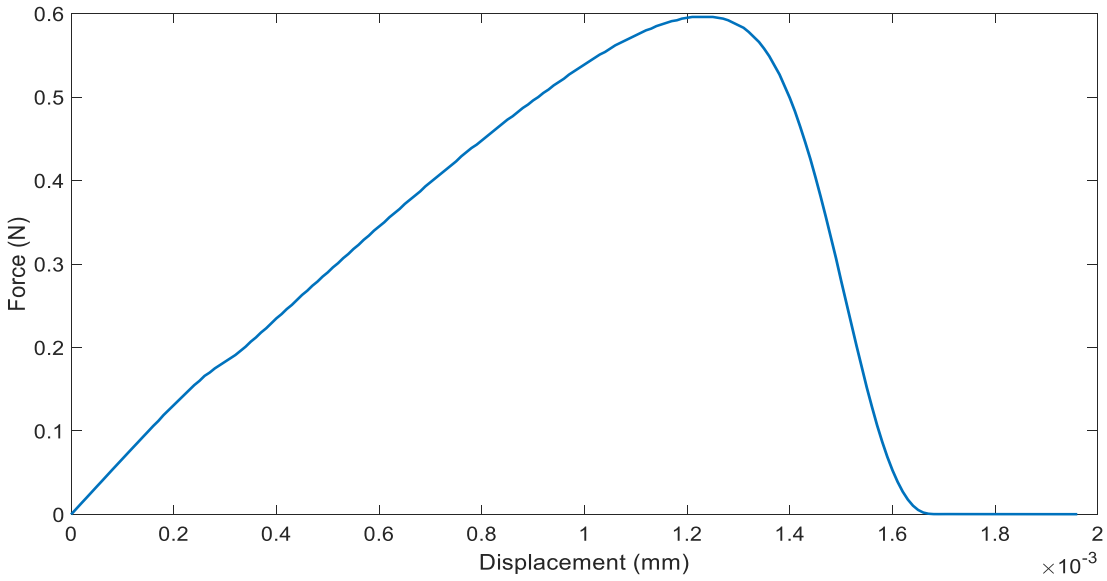

Figure 22:Load-displacement curve for a node adjacent to the moving tool

Fig (22) depicts the obtained load-deflection curve obtained for the process. The steep descent and the smoothed out brutal crack propagation in the post-peak regime distinctively show a non-linear behavior due to induced damage in the model.

5.3 Conclusion

The main outcome of this thesis was to come up with an approach to determine fracture properties of a material using scratch test. This is carried out by bridging the experimental method and the phase field framework. The main conclusions can be categorized in two sets: analytical model and numerical simulation.

5.3.1 Analytical Model

Using the basis of 1-D phase field equations in the presence of experimental findings of scratch test we were able to obtain the fracture property of Eagle Ford shale using an energy-based comparison. An isotropic and rate-independent model is assumed for this purpose. The span of fracture toughness thus obtained depends upon the bounds of material as well as process length scales.

5.3.2 Numerical Simulation

The suggested length scale from analytical model and an averaged-out depth of cut was used to model a two-dimensional replica of the scratch test experiment itself using proper boundary conditions. The assumption was a homogeneous material throughout. Following the work of Molnar et al. (2010) the split scheme operator algorithm was used to solve the phase field and displacement problem. Additionally, as a regularized representation of crack propagation is used no substantial mesh dependence or requirement of enrichment was noticed. The chipping length observed from this model was compared with that of experiments as a way to validate our approach.

5.3.3 Applications, Limitations and Future Perspective

This two-fold procedure combining can be used to obtain a good approximation for fracture toughness of a brittle material based on the collation of scratch-test experimental data and analytical/numerical phase field model. The challenges in terms of rate-dependence, heterogeneity, and anisotropy when it comes to working with rocks still need to be addressed. The advantage of phase field modelling is that they are already being used for heterogenous materials which makes use of direct imaging to update the changing microstructure (Nguyen et al. 2015). Combining this with a 3D modelling of scratch test and indentation can lead to a radical way for determination of fracture properties and identification of the underlying failure mechanism even for strongly heterogeneous and anisotropic materials.

REFERENCES

[1] Abedi, S., Slim, M., & Ulm, F. J. (2016). Nanomechanics of organic-rich shales: the role of thermal maturity and organic matter content on texture. *Acta Geotechnica, 11*(4), 775-787.

[2] Adachi, J. I., Detournay, E., & Drescher, A. (1996). Determination of rock strength parameters from cutting tests. *Proc. NARMS*, 1517-1523.

[3] Akono, A. T., & Ulm, F. J. (2011). Scratch test model for the determination of fracture toughness. *Engineering Fracture Mechanics, 78*(2), 334-342.

[4] Akono, A. T., Reis, P. M., & Ulm, F. J. (2011). Scratching as a fracture process: From butter to steel. *Physical review letters, 106*(20), 204302.

[5] Akono, A. T. (2013). *Assessment of fracture properties and rate effects on fracture of materials by micro scratching: application to gas shale* (Doctoral dissertation, Massachusetts Institute of Technology).

[6] Alehossein, H., Detournay, E., & Huang, H. (2000). An analytical model for the indentation of rocks by blunt tools. *Rock Mechanics and Rock Engineering, 33(4)*, 267-284.

[7] Ambati M. (2017). *Phase-field modelling and computations of brittle and ductile fracture for solids and shells*. (Doctoral dissertation, Technische Universität Braunschweig).

[8] Atkins, T. (2009). *The science and engineering of cutting: the mechanics and processes of separating, scratching and puncturing biomaterials, metals and non-metals*. Butterworth-Heinemann.

[9] ATKINSON, R. H. (1993). Hardness tests for rock characterization. In *Rock Testing and Site Characterization* (pp. 105-117). Pergamon.

[10] Bažant, Z. P., & Pijaudier-Cabot, G. (1989). Measurement of characteristic length of nonlocal continuum. *Journal of Engineering Mechanics, 115*(4), 755-767.

[11] Bieniawski, Z. T. (1974). Estimating the strength of rock materials. *Journal of the Southern African Institute of Mining and Metallurgy, 74*(8), 312-320.

[12] Dubey, V., Abedi, S., & Noshadravan, A. (2018, August). Multiscale Modelling *Mechanics/Geomechanics Symposium*. American Rock Mechanics Association.

[13] Huang, H., & Detournay, E. (2008). Intrinsic length scales in tool-rock interaction. *International Journal of Geomechanics, 8*(1), 39-44.

[14] Irwin, G. R. (1958). Handbuch der Physik. V. VI Elasticity and Plasticity.

[15] Johnson, K. L. (1970). The correlation of indentation experiments. *Journal of the Mechanics and Physics of Solids, 18*(2), 115-126.

[16] Klinsmann, M., Rosato, D., Kamlah, M., & McMeeking, R. M. (2015). An assessment of the phase field formulation for crack growth. *Computer Methods in Applied Mechanics and Engineering, 294*, 313-330.

[17] Kuhn, C., Schlüter, A., & Müller, R. (2015). On degradation functions in phase field fracture models. *Computational Materials Science, 108*, 374-384.

[18] Linse, T., Hennig, P., Kästner, M., & de Borst, R. (2017). A convergence study of phase-field models for brittle fracture. *Engineering Fracture Mechanics, 184*, 307-318.

[19] Marsh, D. (1964). Plastic flow in glass. *Proceedings of the Royal Society of London. Series A. Mathematical and Physical Sciences, 279*(1378), 420-435.

[20] Mashhadian, M., Abedi, S., & Noshadravan, A. (2018). Probabilistic multiscale characterization and modeling of organic-rich shale poroelastic properties. *Acta Geotechnica, 13*(4), 781-800.

[21] Mashhadian, M., Abedi, S., & Noshadravan, A. (2018, August). A Probabilistic Multiscale Approach for Modeling Poromechanical Properties of Shales. In *52nd US Rock Mechanics/Geomechanics Symposium*. American Rock Mechanics Association.

[22] Mashhadian, M., Verde, A., Sharma, P., & Abedi, S. (2018). Assessing mechanical properties of organic matter in shales: Results from coupled nanoindentation/SEM-EDX and micromechanical modeling. *Journal of Petroleum Science and Engineering, 165*, 313-324.

[23] Dal Maso, G. (1993). An introduction to Γ. *Convergence, 8*.

[24] Miehe, C., & Lambrecht, M. (2001). Algorithms for computation of stresses and elasticity moduli in terms of Seth–Hill's family of generalized strain tensors. *Communications in numerical methods in engineering, 17*(5), 337-353.

[25] Miehe, C., Hofacker, M., & Welschinger, F. (2010). A phase field model for rate-independent crack propagation: Robust algorithmic implementation based on

operator splits. *Computer Methods in Applied Mechanics and Engineering, 199*(45-48), 2765-2778.

[26] Miehe, C., Welschinger, F., & Hofacker, M. (2010). Thermodynamically consistent phase-field models of fracture: Variational principles and multi-field FE implementations. *International Journal for Numerical Methods in Engineering, 83*(10), 1273-1311.

[27] Molnár, G., & Gravouil, A. (2017). 2D and 3D Abaqus implementation of a robust staggered phase-field solution for modeling brittle fracture. *Finite Elements in Analysis and Design, 130,* 27-38.

[28] Monfared, S., & Ulm, F. J. (2016). A molecular informed poroelastic model for organic-rich, naturally occurring porous geocomposites. *Journal of the Mechanics and Physics of Solids, 88,* 186-203.

[29] Mumford, D., & Shah, J. (1989). Optimal approximations by piecewise smooth functions and associated variational problems. *Communications on pure and applied mathematics, 42*(5), 577-685.

[30] Nagaraja S. (2017). *Phase-field modeling of brittle fracture with multi-level hp-FEM and the Finite Cell Method*. (Master's Thesis, Technische Universität München).

[31] Nguyen, T. T., Yvonnet, J., Zhu, Q. Z., Bornert, M., & Chateau, C. (2015). A phase field method to simulate crack nucleation and propagation in strongly heterogeneous materials from direct imaging of their microstructure. *Engineering Fracture Mechanics, 139,* 18-39.

[32] Nguyen, T. T., Yvonnet, J., Bornert, M., Chateau, C., Sab, K., Romani, R., & Le Roy, R. (2016). On the choice of parameters in the phase field method for simulating crack initiation with experimental validation. *International Journal of Fracture, 197*(2), 213-226.

[33] Richard, T. (1999). *Determination of rock strength from cutting tests* (Doctoral dissertation, University of Minnesota).

[34] Richard, T., Dagrain, F., Poyol, E., & Detournay, E. (2012). Rock strength determination from scratch tests. *Engineering Geology, 147*, 91-100.

[35] Sargado, J. M., Keilegavlen, E., Berre, I., & Nordbotten, J. M. (2018). High-accuracy phase-field models for brittle fracture based on a new family of degradation functions. *Journal of the Mechanics and Physics of Solids, 111*, 458-489.

[36] Sulem, J., Vardoulakis, I., & Exadaktylos, G. (2001). Microstructural effects in stress concentration and fracture problems in rock mechanics. *Non linear Fracture and Damage Mechanics, WITPress*, 161-199.

[37] Szwedzicki, T. (1998). Indentation hardness testing of rock. *International Journal of Rock Mechanics and Mining Sciences, 35*(6), 825-829.

[38] Ulm, F. J., & Abousleiman, Y. (2006). The nanogranular nature of shale. *Acta Geotechnica, 1*(2), 77-88.

[39] Zhou, Y., & Lin, J. S. (2014). Modeling the ductile–brittle failure mode transition in rock cutting. *Engineering Fracture Mechanics, 127*, 135-147.

APPENDIX A

FINITE ELEMENT ALGORITHM

A split scheme operator is used to solve the two-dimensional phase-field fracture problem. The following system of equation is solved using Newton Raphson method, which updates the tangent matrix and residue vector after each iteration.

$$\begin{bmatrix} \boldsymbol{K_d^n} & \mathbf{0} \\ \mathbf{0} & \boldsymbol{K_u^n} \end{bmatrix} \begin{Bmatrix} \boldsymbol{d_{n+1}} \\ \boldsymbol{u_{n+1}} \end{Bmatrix} + \begin{Bmatrix} \mathbb{R}_d^n \\ \mathbb{R}_u^n \end{Bmatrix} = \mathbf{0} \tag{A. 1}$$

The tangent stiffness matrices for phase field and displacement are calculated as follows:

$$\boldsymbol{K_d} = \int_{\Omega} \left\{ \left({}^{G_C}/_{l} + 2H \right) \boldsymbol{N_d}^{\boldsymbol{T}} \boldsymbol{N_d} + G_C l \boldsymbol{B_d}^{\boldsymbol{T}} \boldsymbol{B_d} \right\} \mathrm{d}\Omega \tag{A. 2}$$

$$\boldsymbol{K_u} = \int_{\Omega} \{(1-d)^2 + k\} \boldsymbol{B_u^T C_0 B_u} \, d\Omega \tag{A. 3}$$

Where N_d and N_u are the shape function vectors and B_d and B_u are the shape function derivatives matrix of phase field and displacement, respectively. The phase field and its gradient can be approximated in one element as: $d = \boldsymbol{N_d d}_i$ and $\nabla d = \boldsymbol{B_d d}_i$, where $\boldsymbol{d}_i$ are the nodal values. Similarly, the FE approximations for displacement is $u = \boldsymbol{N_u u}_i$. The strain history functional (H) is calculated as per Eq. (22) for each element and in every iteration. The residual vectors are computes as:

$$\mathbb{R}^d = \int_{\Omega} \left\{ \left(\frac{G_C}{l} d - 2(1-d)H \right) \boldsymbol{N_d^T} - G_C l \boldsymbol{B_d}^{\boldsymbol{T}} \nabla d \right\} \mathrm{d}\Omega \tag{A. 4}$$

$$\mathbb{R}_{\boldsymbol{u}} = \int_{\boldsymbol{\Omega}} ((\mathbf{1}-\boldsymbol{d})^2 + \boldsymbol{k}) \boldsymbol{B_u^T \sigma_0} \, \boldsymbol{d\Omega} - \int_{\boldsymbol{\Omega}} \boldsymbol{N_u^T f} \, \boldsymbol{d\Omega} - \int_{\boldsymbol{\partial\Omega_F}} \boldsymbol{N_u^T \bar{F}} \, \boldsymbol{d\Gamma} \tag{A. 5}$$

Where $\boldsymbol{\sigma_0} = \boldsymbol{C_0 \varepsilon}$ and $\bar{\boldsymbol{f}}, \bar{\boldsymbol{F}}$ are prescribed Neumann boundary conditions on the body.

APPENDIX B

ANALYTICAL ALGORITHM